Optical Orientation Determination for Airborne and Spaceborne Line Cameras

Methoden der optischen Orientierungsbestimmung für flugzeug- und satellitengestützte Zeilenkameras

D I S S E R T A T I O N

zur Erlangung des akademischen Grades

Dr. rer. nat.
im Fach Informatik

eingereicht an der Mathematisch-Naturwissenschaftlichen Fakultät II
der Humboldt-Universität zu Berlin

von
Dipl.-Inf. Jürgen Wohlfeil

Präsident der Humboldt-Universität zu Berlin:
Prof. Dr. Jan-Hendrik Olbertz

Dekan der Mathematisch-Naturwissenschaftlichen Fakultät II:
Prof. Dr. Elmar Kulke

Gutachter:
1. Prof. Dr. Beate Meffert
2. Prof. Dr. Ralf Reulke
3. Prof. Dr. Stephan Nebiker
4. Prof. Dr. Bodo Rosenhahn

eingereicht am: 12. April 2011
Tag der mündlichen Prüfung: 11. Oktober 2011

Abstract

Airborne and spaceborne line cameras allow a very economic acquisition of high-resolution and wide swath images of the Earth. They generate two-dimensional images while rotating or translating, which causes a non-rigid image geometry. Non-uniform motion of the camera can negatively affect the image quality. Due to this, a key requirement for line cameras is that fast orientation changes have to be avoided or measured with a very high rate and precision. Camera stabilization is not always possible and can often only be achieved with very high effort. In such cases it is essential to measure the camera's orientation accurately to ensure that the resulting imagery products can be geometrically corrected in a later processing step. Adequate high-end measurement systems are large and expensive and their angular and temporal resolution can be still too low for many possible applications. Due to these reasons there is great interest in approaches to support the orientation measurement by using optical information received through the main optics or telescope.

In this thesis two different approaches are presented that allow the determination of a line camera's orientation changes optically. In addition to this the determined orientation changes can be used to derive the precise absolute orientation of an unstabilized airborne line camera.

One approach to determine fast orientation changes is based on small auxiliary frame image sensors, mounted on the focal plane of the main camera or behind separate optics. The optical flow on these sensors is determined by tracking suitable image features through a series of images. It is shown that this can be performed onboard and in real time using a standard CPU. From the optical flow the orientation changes of any remote sensing system can be derived.

The second approach does not require any additional sensors to determine orientation changes. It relies only on the images of a line camera and a rough estimate of its trajectory by taking advantage of the typical geometry of multi-spectral line cameras. In a first step homologous points are detected within the distorted images of different spectral bands. These points are used to calculate the orientation changes of the camera with a high temporal and angular resolution via bundle adjustment.

Finally it is shown how the absolute exterior orientation of an airborne line camera can completely be derived from the optically determined orientation changes. The orientation changes are used to pre-correct the line images, in which homologous points can reliably be determined using an image feature detection and description algorithm. Together with position measurements these points are used to determine the precise absolute orientation via bundle adjustment of a block of overlapping line images.

Keywords: Remote Sensing, Photogrammetry, Linecamera, Optical Flow, Orientation Determination, Navigation

Zusammenfassung

Flugzeug- und satellitengestützte Zeilenkameras ermöglichen eine sehr ökonomische Aufnahme von hoch aufgelösten Luftbildern mit großer Schwadbreite. Sie erzeugen zweidimensionale Bilder durch Rotation oder Translation, wodurch eine nicht starre Bildgeometrie zustande kommt. Eine ungleichförmige Bewegung der Kamera kann sich auf die Bildqualität auswirken. Deswegen ist es unerlässlich, schnelle Orientierungsänderungen der Kamera während der Aufnahme zu vermeiden oder mit angemessener Genauigkeit und Messrate zu erfassen. Leider ist eine Stabilisierung der Kamera nicht immer möglich oder mit inakzeptabel hohem Aufwand verbunden. In solchen Fällen ist es unerlässlich, die Orientierung genau zu messen, um sicher zu stellen, dass die resultierenden Bilder in einem Nachbearbeitungsschritt geometrisch korrigiert werden können. Angemessene High-End-Navigationssysteme sind groß und teuer und ihre Genauigkeit und Messrate dennoch für viele denkbare Anwendungen unzureichend. Aus diesen Gründen besteht ein großes Interesse an Methoden zur Unterstützung der Orientierungsmessung durch die Nutzung optischer Informationen vom Hauptobjektiv bzw. Teleskop.

In dieser Arbeit werden zwei unterschiedliche Verfahren vorgestellt, die es erlauben, schnelle Orientierungsänderungen der Kamera auf optischem Wege zu ermitteln. Außerdem wird gezeigt, dass anhand dieser Orientierungsänderungen die präzise absolute Orientierung einer unstabilisierten Luftbildkamera ermittelt werden kann.

Eines der beiden Verfahren zur Bestimmung von schnellen Orientierungsänderungen basiert auf zusätzlichen Bildsensoren mit kleiner Fläche. Diese können auf der Fokalebene der Hauptkamera oder hinter separaten Objektiven angebracht sein. Der optische Fluss auf diesen Bildsensoren wird durch die Verfolgung passender Bildmerkmale durch eine Serie von Bildern ermittelt. Es wird gezeigt, dass dies mit einer Standard-CPU an Bord in Echtzeit durchgeführt werden kann. Anhand des optischen Flusses können die Orientierungsänderungen beliebiger Fernerkundungssysteme abgeleitet werden.

Das zweite Verfahren benötigt zur Ermittlung der Orientierungsänderungen keine zusätzlichen Sensoren oder Rechenkapazitäten an Bord. Es beruht ausschließlich auf den Inhalten der Zeilenbilder und der gemessenen Kameratrajektorie. Hierfür macht sich das Verfahren die typische Geometrie multispektraler Zeilenkameras zu Nutze. Zunächst werden homologe Punkte in den möglicherweise stark verzerrten Zeilenbildern unterschiedlicher Spektralbänder extrahiert. Diese Punkte werden dann dazu benutzt, die Orientierungsänderungen der Kamera über einen Bündelblockausgleich zu ermitteln.

Schließlich wird gezeigt, dass es möglich ist, die absolute Orientierung einer luftgestützten Zeilenkamera anhand der optisch ermittelten Orientierungsänderungen hochgenau zu ermitteln. Die bekannten Orientierungsänderungen werden dabei zur weitgehenden Entzerrung der Zeilenbilder genutzt. Mit einem Algorithmus zur Erkennung und Zuordnung von Bildmerkmalen können in diesen Bildern homologe Punkte zuverlässig gefunden werden. Zusammen mit den Positionsmessungen werden diese Punkte dazu benutzt, für einen großen Block überlappender Bilder die absolute Orientierung mithilfe eines Bündelblockausgleichs zu ermitteln.

Schlagworte: Fernerkundung, Photogrammetrie, Zeilenkamera, Optischer Fluss, Orientierungsbestimmung, Lagemessung

Contents

1 Introduction

1.1 Motivation

Airborne and spaceborne images provide valuable information of the Earth's entire surface. Although it has already been photographed many times there is still a strong demand for contemporary images with increasing spatial, spectral and radiometric resolution. The reason for this is that they are essential for many applications in cartography, vegetation analysis, land-use planning, etc. One example is the monitoring of the clearance of rain forest, as presented by Almeida-Filho and Shimabukuro [2002]. Like many others, this study makes use of a time series of multispectral satellite imagery which enables automatic change detection. Another example for the importance of very recent spaceborne imagery is its role at large scale disasters. The earth quake in Haiti in 2010 (ScienceDaily [2010]) and the wide flooding in Australia in 2011 are only two of over 200 activations of the International Charter "Space and Major Disasters" (Stryker and Jones [2009]) since 1999. By providing a good overview of the current situation it highly supports fast and effective help.

The images are taken by remote sensing systems equipped with different types of sensors. They can be divided into two groups, the group of active sensors and the group of passive sensors. Active sensors emit a signal and analyze the reflected or re-emitted part of it. Examples for such sensors are radar (radio detection and ranging) and lidar (light detection and ranging), which are widely used in remote sensing. Passive sensors only detect naturally occurring energy. This energy is, in the case of remote sensing, electromagnetic radiation ranging from thermal infrared to ultraviolet light. There are passive imaging sensors sensible to different wave lengths of the electromagnetic spectrum. By using suitable filters or diffraction grating multiple sensors of the same type can be used to measure the radiation in different narrow bands of the electromagnetic spectrum.

There are three basically different techniques to capture (two-dimensional) images with such sensors. One technique is to use one single sensor and sequentially scan the Earth's surface point by point with it. Higher scan rates can be achieved with sensors consisting of multiple photodetectors arranged in a one- or two-dimensional array. These two techniques are mainly used for passive sensors and more closely described in the following.

Sensors with a two-dimensional array of photodetectors (called frame sensors in the following) are able to capture an entire image at a time. The resolution of such frame sensors is very limited as the amount of necessary photodetectors increases as the square of the image width. In order to retrieve multispectral images usually multiple frame sensors are used in airborne cameras. Each frame sensor is equipped with different filters and must be placed behind a separate optics in order to capture the same area

as the others. This does not only rise the costs, weight and size of the camera but also makes its geometry and the geometric calibration very complex (Smith et al. [2010]). Moreover this means that frame sensors are not suitable for high resolution remote sensing satellites because the use of multiple telescopes is even less economical as in the airborne case. Another option is the usage of one single sensor with a mosaic of filters causing different photodetectors to be sensitive to different spectral bands, according to Bayer [1976]. Unfortunately, this technique is linked with a loss of spatial resolution when increasing the spectral resolution. Another type of sensor avoids this disadvantage by using vertically stacked photodiodes sensible for different wavelengths (Merrill [1999]). As shown by Leberl et al. [2002] such a sensor has many advantages compared to sensors with a mosaic of filters. But for high resolution and multispectral imaging this type of sensor can currently not compete with other sensors due to its low resolution and limited number of spectral bands.

An alternative to frame sensors is to use line sensors having only one line of photodetectors. Such sensors make use of the movement of the camera to scan the surface of the earth line by line. In contrast to frame sensors the number of photodetectors increases linearly with the image width and allows the fabrication of sensors with a very high resolution at relatively low costs. Multispectral images can be captured through one single optics by placing multiple sensors with different spectral sensitivities in parallel on the focal plane (Petrie [2005] provides a good overview of different types of line cameras). Two line sensors with the same spectral sensitivity can also be staggered, as found for example in the aerial line camera ADS (Eckardt et al. [2000], Reulke et al. [2004]) and the HRS (high resolution stereo) sensors of the SPOT satellites (Riazanoff [2004]). This technique is used to increase the resolution of the camera by shifting two narrow and parallel sensor arrays by half a pixel.

If a line camera is translated with constant speed and the rotation is held constant then the resulting line image has a simple geometry (Fig. 1.1b): In scanning direction the image is the result of a parallel projection and in line direction it is a perspective projection. Especially when operating aerial line cameras a non-linear movement and permanent changes in the camera's orientation (attitude) cannot be avoided. This results in a very complex geometry where basically every line of the image can have a different orientation. In Fig. 1.1c such a geometry is displayed. As an example a real uncorrected airborne line image is shown in Fig. 1.2a. The image can only be used if the position and orientation of the camera is measured adequately during the scan. Having this information, every line of the image can be projected onto a virtual planar surface or a digital surface model. This way all distortions of the image can be removed, as shown in Fig 1.2b.

To measure the position and orientation (exterior orientation) of remote sensing cameras it is not only necessary to be able to compensate the distortions in line images. Together with the geometric calibration (interior orientation) of the camera this information is mandatory for the direct georeferencing of the images. This is essential for the geometric interpretation of the images, required by almost all of their applications.

The effort to measure the exterior orientation of a line camera during the scan depends on the carrier and its dynamics. The measurement of the position is relatively uncritical

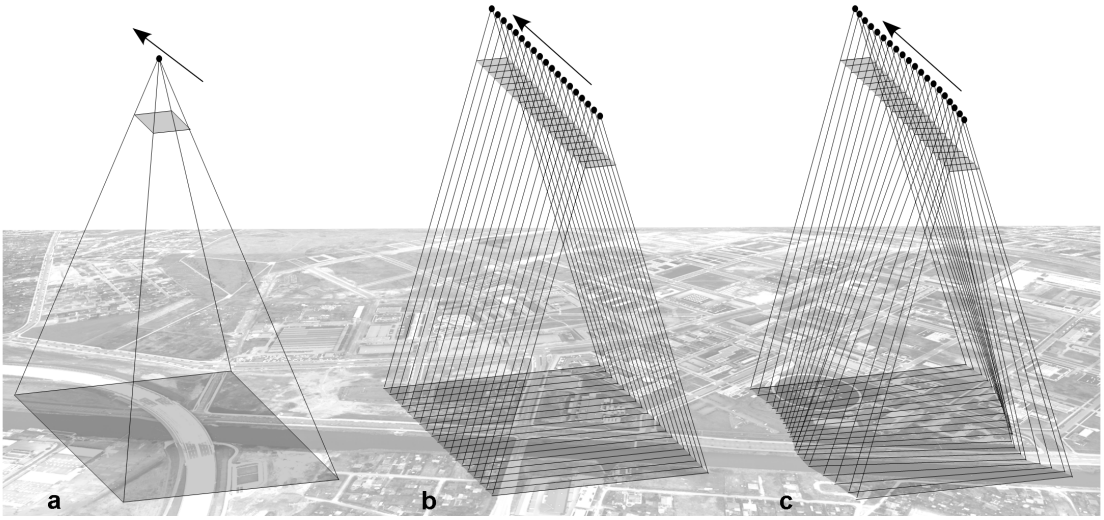

Figure 1.1: The geometry of different types of images. The focal plane (upper dark area) is flipped in front of the center of projection (small dot). The arrow indicates the direction of flight. a: Frame image. b: Ideal line image. c: Real line image

in both, the airborne and spaceborne case. An aircraft (and so the camera) does not change the translation speed by a relevant amount between the capture of two subsequent lines. This is due to its high mass with respect to the very short line intervals. Therefore it is not necessary to measure its position with a high rate. The position of a satellite is almost perfectly predictable and its motion very linear. In contrast to this, the orientation measurement is much more critical.

The orientation of an aircraft is affected by turbulences and maneuvers the pilot has to perform to retain control over the aircraft and follow a straight flight path (Fig. 1.2). Moreover, vibrations of the aircraft caused by the engine and high frequency components of air turbulences lead to short-term orientation changes of the camera. They cause significant orientation changes with frequencies (Fig. 3.2c). Especially, these fast orientation changes are very difficult to measure and can cause an almost independent orientation of every single captured line. Their effect can be reduced by isolating the camera from the aircraft's motion as far as possible. Even though this is related to a high additional effort it is a widely-used solution for this problem. An alternative way is to allow and to measure fast orientation changes of the camera. This way their effects on the images can then be corrected later. But the adequate measurement of the orientation is challenging for modern line cameras with increasing line rate and angular resolution, even for specialized high-end measurement systems.

Spaceborne remote sensing cameras usually consist of a large telescope whose orientation is influenced by necessary movements of reaction wheels, antennas, solar panels, cooling systems etc. of the satellite. Even if these actors can be switched off during

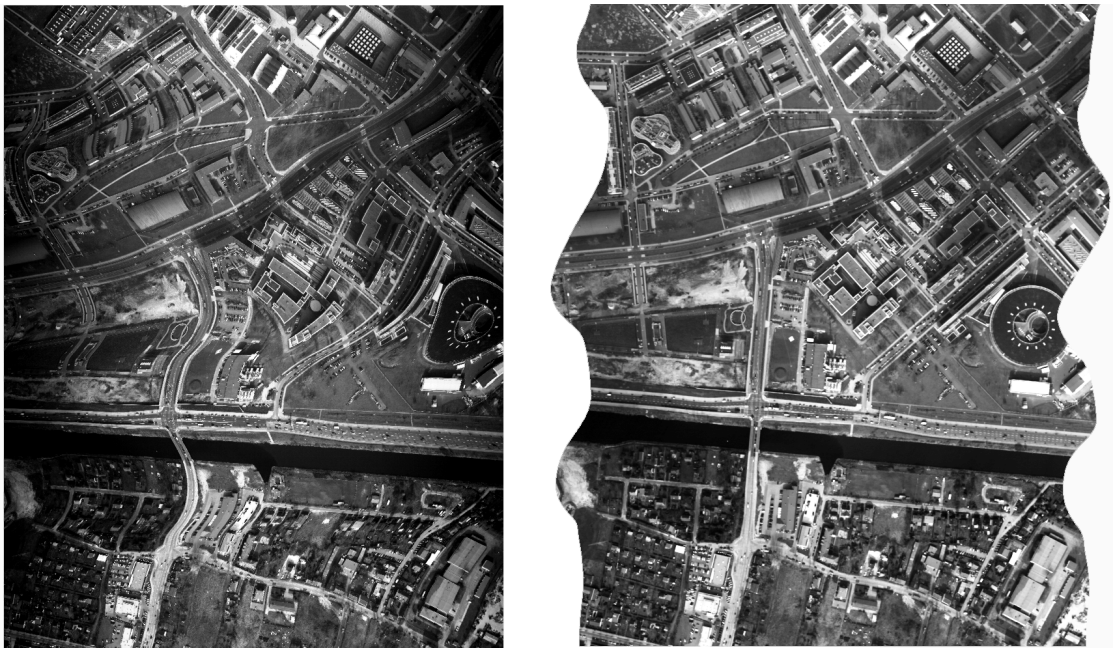

Figure 1.2: The uncorrected (left) and the corrected (right) version of an aerial line image. A detailed view of a small section is shown in Fig. 3.2a and c.

image acquisition it takes a certain time until the oscillation of the whole satellite drops below an acceptable magnitude. This waiting period means wasting time and reduces the efficiency of the satellite a lot. Satellites that continuously scan images cannot even use this technique. Due to their large extents, the stabilization of satellite based line cameras is very difficult and expensive, if possible at all.

Even though it can be very challenging, the ability to accurately measure fast orientation changes of airborne and spaceborne line cameras has many benefits. It offers a chance to reduce or completely save the effort for an extensive stabilization of the camera. This enables the use of high resolution remote sensing cameras with very economic and ecologic lightweight aircrafts, for example. It also could help to operate remote sensing satellites more efficiently and increase their agility.

Due to these reasons in this thesis solutions are sought that allow the measurement of orientation changes with an appropriately high rate and precision. This must be achieved with very little additional effort in order to gain a clear advantage compared to the avoidance of fast orientation changes.

As the resolution and line rate of line cameras is steadily increasing, the orientation measurement techniques must also be improved continuously. Therefore it is desirable that the achieved temporal and angular resolution increases according to rising line rates and resolutions of future cameras.

In the two following Sections established techniques for orientation measurement are

presented and alternative approaches are shown and discussed. After that, the research question of this thesis is presented and the approaches to answer the question are discussed.

1.2 Orientation Measurement for Line Cameras

While the position measurement of airborne and spaceborne cameras mainly or completely relies on a Global Navigation Satellite System (GNSS) the measurement of its orientation is typically based on an Inertial Measurement Unit (IMU). An IMU has three orthogonally oriented gyroscopes and accelerometers. Together with the position measurements the accelerometers and gyroscopes allow the determination of the absolute orientation of airborne cameras. Remote sensing satellites use additional sensors like star and sun trackers. But in both cases the accurate measurement of mid-term and short-term orientation changes is based on the gyroscopes if they can be measured at all.

Due to their importance for the measurement of the camera's orientation different types of gyroscopes are described in brief. A good overview of the current development of gyroscopes is given by Schmidt [2010].

The first generation of gyroscopes was based on rotating masses whereas the most common contemporary type is the vibrating structure gyroscope. As the name suggests it is based on the physical principle that a vibrating object keeps vibrating in the same plane of motion even if its support rotates. The palette of implementations ranges from inexpensive miniature models up to high-end products. A big advantage of vibrating structure gyroscopes is that the angular rate can be measured with high accuracy. On the other hand they are very sensible to environmental influences like temperature and air pressure. High-end versions try to keep these influences constant to provide a high bias stability. But other types of gyroscopes achieve a much higher bias stability and therefore a lower drift over time. The frequency of vibration is the main limiting factor of the gyroscope's bandwidth. The bandwidth restricts the temporal resolution of the measurement of angular rates. An increased bandwidth is usually related to a decreased long-term stability.

Fiber optic gyroscopes make use of the Sagnac effect to determine angular rates. Two light beams of the same light source travel along a looped fiber in opposite directions. If the system rotates around the axis of the loop one beam needs more time to travel through the fiber than the other. This has an effect on the interference of the two recombined beams that can be measured. High-end fiber optic gyroscopes achieve a very high angular and temporal resolution by increasing the Sagnac effect with a very high number of fiber loops. Unfortunately, the required length and quality of the fibers make such models very expensive. Even though recent models also reach a good bias stability fiber optic gyroscopes have a high noise level (gyro angle random walk), compared to other types of gyroscopes of the corresponding price segment.

Another type of gyroscope is the ring laser gyroscope. It also uses the Sagnac effect but rather than the fiber optic gyroscope the ring is part of the laser. It has a much lower

drift and noise than other types of gyroscopes but the achievable angular resolution is generally very low. Therefore, even high-end models are not suitable to directly measure the orientation of remote sensing cameras. Another disadvantage is that they are even more expensive than the fiber optic gyroscopes.

For modern remote sensing satellites the accuracy of any of these types of gyroscopes is accurate enough to achieve a pointing accuracy in the range of the ground sampling distance. This is due to the very high angular resolution necessary to achieve ground sampling distances down to half a meter from several hundreds of kilometers of distance.

For high resolution airborne cameras mainly high-end vibrating structure gyroscopes and fiber optic gyroscopes are used. They are very expensive but meet the requirements if the camera is isolated from the fast orientation changes of the aircraft. This is achieved with a gyro-stabilized camera mount that uses hydraulic or electromechanical components to keep the orientation of the camera constant while the aircraft moves. This active part of camera stabilization is controlled by the measurements of a built-in or external IMU and can only compensate a limited spectrum of orientation changes. Therefore it is mandatory to passively damp the high-frequent components that cannot be compensated as well as possible. This can be achieved by installing mechanical dampers between the aircraft and the camera mount or by inserting a vibration isolation ring between the camera mount and the camera.

Especially for line cameras the need for extensive camera stabilization is primarily a consequence of the limited measurement rate of the gyroscopes. As the line rates and resolutions of line cameras increase constantly orientation measurement will presumably continue being a major challenge in the context of line cameras in the future.

Due to these difficulties first alternative approaches for orientation measurements have been developed very early. One of these approaches is the star tracker. By means of additional telescopes directed into deep space the stars can be tracked to determine the orientation of a satellite (Eisenman et al. [1997]). With the help of a star catalogue even the absolute orientation can be determined with this approach. Unfortunately, star trackers would need very large telescopes to be able to determine the orientation with the resolution of the main camera. Also their measurement rate is relatively low (in the range of a few measurements per second). This is due to the long exposure times required to capture the stars. Their luminance is about 6 orders of magnitude lower than the luminance of the Earth's surface at daytime. Even if star trackers would have a similar sensitivity as the main sensor this makes it impossible to capture them with a similar rate.

For aircrafts star trackers can, of course, not be applied. Also the tracking of the sun is unreliable due to possible high clouds and does not allow the measurement of all three degrees of freedom. Another problem is that the corresponding sensor would have to be installed at the top of the aircraft, being physically too isolated from the vibrations of the camera to measure them accurately.

Another way to measure the orientation of an airborne or spaceborne line camera optically is to use the optical information received by the main optics. It may use the images of auxiliary sensors mounted on the focal plane of the camera as well as the images of the primary sensor(s). This version of orientation measurement is of high

interest because it allows very economic solutions that achieve precise results, especially when measuring fast orientation changes. The approaches presented in this thesis make use of this principle.

Due to the great advantages of optical orientation measurement for line cameras various work has been done in this field. The following section gives an overview about the most important approaches related to this thesis.

1.3 Related Work

Already in the eighties Otto Hofmann [1984, 1988a] claimed that it is possible to derive the exterior orientation of a three-line camera from its images. In 1988 he patented an approach based on the manual selection of ground control points. With an automated bundle adjustment that used these points the camera's exterior orientation could be calculated (Hofmann [1988b]). The exterior orientation of the camera was modeled by multiple sets of exterior orientation parameters. These so-called 'orientation points' were interpolated for the time periods between them. A few years later automatic extraction of homologous points (tie points) became possible (Olhof [1995]). The absolute orientation could be improved by using a mixture of homologous points and a few ground control points (Haala et al. [1997], Cramer et al. [1997]).

A new generation of very precise navigation systems enabled direct georeferencing with a gradually increasing precision (Schwarz et al. [1993], Cramer [1999]). These systems combine a high-end IMU with a newly available NAVSTAR GPS (Global Positioning System) receiver. They allowed the direct measurement of the camera's absolute exterior orientation without requiring any homologous points or ground control points. Unfortunately, such high-end systems are very expensive and their accuracy is limited. Many new approaches combine GPS/IMU based navigation data with automatically extracted homologous points. These approaches are not only used for the aerial three-line cameras like the ADS40 (Hinsken et al. [2002]) and STARIMAGER (Gruen and Zhang [2002], Kocaman [2005]). Also the measured exterior orientation of spaceborne line cameras has to be improved in order to achieve the accuracy required for many applications (Li et al. [2002], Jama et al. [2009]). This applies also to the spacecraft mars express with the line camera HRSC (Spiegel [2007], Schmidt et al. [2008], Gwinner et al. [2009]).

All these approaches require the camera to be stabilized to avoid orientation changes with frequencies that are not far below the line rate. Without exactly knowing the temporal distance between the Hofmann's 'orientation points' it can be assumed that it was in the order of seconds. The computational power of the computers of his epoch and the effort for the selection of homologous points would not allow more complex models. However, the demands on the geometrical accuracy of airborne imagery were much lower in those times.

Even though the image based orientation determination techniques improved a lot in the past few years line cameras still need to be stabilized with high effort. This way the orientation of the camera changes only slightly and slowly and the resulting distortions of the images are small and smooth. The main reason for this is that the distortions

caused by fast orientation changes are a serious problem for the automatic extraction of homologous points from line images. On the other hand these points are mandatory to determine the orientation changes, as it is addressed more precisely in Section 1.4.

One way to handle the problem was presented by Janschek and Tchernykh [2001] and Janschek et al. [2005]. The approach is based on the optical flow measured with two additional frame sensors. They are mounted at the focal plane of a camera next to the main line sensor(s). The optical flow on the frame sensors is supposed to be equivalent to the optical flow on the main line sensor(s).

After the optical flow has been extracted from the images of the frame sensors it can be used for two purposes. It can be transmitted or stored in order to compensate the effects of fast orientation changes on the main images in a following processing step. But it can also be used to move the focal plane according to the optical flow to compensate the orientation changes directly. The second version could be regarded as a technique of camera stabilization. In any case the effects of fast orientation changes are only indirectly measured and corrected as shifts of the focal plane. For small rotation angles this assumption is very reasonable and simpler than modeling the actual spatial rotations of the camera.

Vibrations of a satellite or a spacecraft can also be measured via optical information from the main line sensors. A big advantage of such approaches is that they don't require any additional hardware or bandwidth. As shown by de Lussy et al. [2008], harmonic oscillations of the SPOT 5 satellite can be determined optically in the images of its main line sensors. This is possible due to the typical multi-spectral line camera geometry of this satellite. By maximizing the correlation of small image windows of the different spectral bands, the frequencies and amplitudes of four different harmonic oscillations are determined. This principle of determining fast orientation changes is very promising. For particular applications with only this distinct type of vibration it is a very good solution. For many other applications the model of possible orientation changes is too restricted.

Very recently Perrier et al. [2010] presented an approach that models the vibrations of the orientation of the spacecraft with piecewise polynomial interpolation. This model is expected to allow the correction of a wider range of orientation changes than the model of de Lussy et al. it refers to. The polynomials are iteratively estimated via an iterative image registration method. A basic test of the algorithm on simulated satellite imagery showed that the approach allows to reduce the effects of vibrations in the image. The major difficulty seems to be the choice of the temporal distance between the pieces of polynomials. In order to correct the low frequency components of the vibrations the distance had to be set to 20 time samples. At the same time this prevents the adequate modeling of the high frequency components of the vibrations. The corrections only apply to the roll and pitch angle of the spacecraft. The effects of the vibrations to the yaw angle are proposed to be negligible, which is reasonable due to the geometry of spaceborne cameras.

1.4 Research Question and Approaches

From all of the above-mentioned approaches the approach of Janschek et al. is the only one without fundamental limitations of the frequency of measurable orientation changes. The actually limiting factor is the frame rate of the auxiliary frame sensors which can be very high for small sensors. The additional effort necessary for the frame sensors and the online extraction of the optical flow are relatively low but still considerable.

The line image based approaches avoid this effort but restrict the range of correctable orientation changes drastically. As a consequence of that they can only be used in special cases.

In order to find ways to overcome these restrictions the main research question of this thesis is: *How can the orientation of a line camera be measured optically with high angular and temporal resolution and a minimum of technical effort?*

Theoretically this would be possible for a three-line camera with a classical bundle adjustment using automatically extracted homologous points. If the position of the camera is measured the scale and offset to an absolute geographic coordinate system is given. This means that there is no need to use additional ground control points to determine the absolute orientation of the camera. Every line could be regarded as a single image with an individual orientation. If there are enough homologous points connecting intersecting lines the orientation parameters of every single line could be determined via bundle adjustment. Unfortunately, there are two major problems to implement this approach.

The first problem is that the automatic selection of homologous points in uncorrected line images is difficult if the camera's orientation changes quickly during the scan of the images. If the absolute orientation it not known with high accuracy it cannot be predicted exactly where a point in one image is located in the other images. As a consequence, the assignment of corresponding image points is very ambiguous.

The second problem is that fast orientation changes distort object points in different images in different ways. This makes corresponding points look different and makes it almost impossible to assign them correctly.

Assuming that the necessary number of homologous points could be found for every line a second problem appears. The bundle adjustment needed to calculate the orientation of all lines would not be solvable in practice. Already the images of small targets consist of hundreds of thousands or even millions of scanned lines. About two to three times as many homologous points would be needed to interlink them. This would result in huge linear equation systems that are by far not solvable in a reasonable amount of time.

Due to these limitations the main goal, to determine the orientation parameters for every single line, is divided into two subsequent steps. In a first step only changes of the camera's orientation are determined. Two different approaches are presented to determine these orientation changes via optical information for different remote sensing systems.

One approach to determine fast orientation changes is based on small auxiliary frame image sensors, mounted on the focal plane of the main camera or behind separate optics.

The optical flow on these sensors is determined by tracking suitable image features through a series of images. It is shown that this can be performed onboard and in real time using a standard CPU. From the optical flow the orientation changes of any remote sensing system can be derived.

The second approach does not require any additional sensors to determine orientation changes. It relies only on the images of a line camera and a rough estimate of its trajectory, taking advantage of the typical geometry of multi-spectral line cameras. In a first step homologous points are detected within the distorted images of different spectral bands. These points are used to calculate the orientation changes of the camera with a high temporal and angular resolution via bundle adjustment.

The determined orientation changes contain small errors that sum up over time preventing a precise long-term measurement of the orientation. But they can be used to pre-correct the line images. On the base of these pre-corrected line images homologous points can be extracted in areas where two or more images overlap. With their help the absolute orientation of the camera can finally be calculated by a global bundle adjustment. As only offsets and long-term drifts of the integrated orientation changes have to be determined the computational complexity of the resulting bundle adjustment is low enough to be solvable.

Another option to determine the absolute orientation is to use conventional measurement systems with a low measurement rate. This way the offsets and long-term errors of the integrated orientation changes can be corrected. An overview of possible combinations of the approaches and the required sensors is given in Figure 1.3.

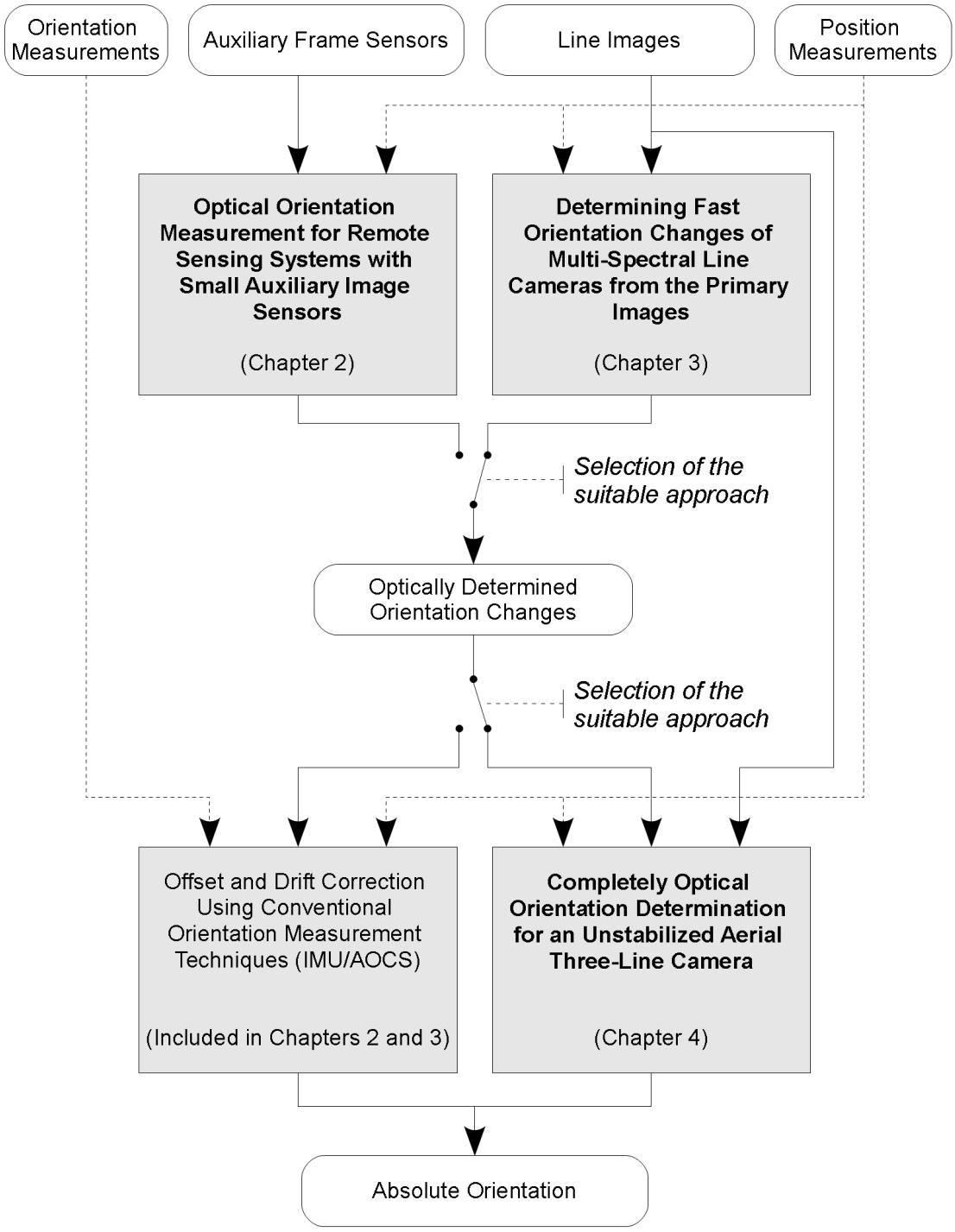

Figure 1.3: Overview of the main chapters of the thesis. Possible combinations of the approaches are shown as switch symbols

1.5 Structure of the Thesis

This thesis has three main Chapters (2 - 3). Chapters 2 and **??** address the optical determination of fast orientation changes in two different ways. In Chapter 3 it is shown how the determined orientation changes can be used to derive the absolute orientation of an airborne three-line camera. The results of the main chapters are summarized and discussed in Chapter 4.

The three main chapters consist of the following publications:

Chapter 2: Jürgen Wohlfeil and Anko Börner. Optical orientation measurement for remote sensing systems with small auxiliary image sensors. *International Archives of the Photogrammetry, Remote Sensing and Spatial Information Sciences*, volume XXXVIII, part 1, 2010.

Chapter **??**: Jürgen Wohlfeil. Determining fast orientation changes of multispectral line cameras from the primary images. *To be published as an article in the ISPRS Journal of Photogrammetry and Remote Sensing*, 2011.

Chapter 3: Jürgen Wohlfeil. Completely optical orientation determination for an unstabilized aerial three-line camera. *In Proceedings of SPIE Sensors, Systems, and Next-Generation Satellites XIV*, Vol. 7826, 2010.

The publications are included in this thesis with the kind permission of the corresponding journal and conference proceedings. Only their layouts and bibliography were unified with the other parts of the thesis.

2 Optical Orientation Measurement for Remote Sensing Systems with Small Auxiliary Image Sensors

Jürgen Wohlfeil[1] and Anko Börner[2]

[1]Humboldt-Universität zu Berlin
Department of Computer Science
Rudower Chaussee 25, 12489 Berlin, Germany

[2]German Aerospace Center
Institute of Robotics and Mechatronics
Rutherfordstr. 2, 12489 Berlin, Germany

juergen.wohlfeil@dlr.de, anko.boerner@dlr.de

Abstract

The accurate measurement of the exterior orientation of remote sensing systems is essential for the quality of the resulting imagery products. Fast orientation changes of the camera immediately before, during or after image acquisition are still serious problems in aerial and satellite based remote sensing. This is due to the fact that in many cases such orientation changes can neither be suppressed effectively nor measured adequately with conventional technology at reasonable costs. In this article, an approach for an auxiliary orientation measurement system is presented that is able to measure a remote sensing system's orientation changes with both, a very high rate and appropriate precision. Two or more auxiliary image sensors are used to measure the orientation changes on the basis of the shift in their images. It is shown that these shifts can be determined by tracking suitable point features through a series of images in real time using a standard mobile CPU for up to 480 images per second. From these shifts the orientation of the whole system can be derived and offset-corrected by conventional orientation measurements. The approach was tested on a test flight with the DLR's MFC line camera and two auxiliary high-speed CMOS cameras. The results are presented and compared to the reference measurements of a high-end INS/GPS system.

2.1 Introduction

The demand for cost-efficient aerial and satellite imagery with high resolution and exact georeferencing is growing steadily. The stabilization of the camera and the measurement of its exterior orientation are key problems in meeting this demand. Due to the high resolution of today's imaging systems, their exterior orientation has to be measured with high precision to ensure the quality of the imaging products. Especially the measurement of the orientation with a high angular and temporal resolution is vital for many line-camera and/or laser scanner based systems due to their increasing angular resolution and scan rates. But conventional exterior orientation measurement systems that meet these requirements are usually too expensive, too large, too heavy or need too much power to allow smart and cost-efficient solutions.

A promising approach to overcome this problems is the compensation of fast orientation changes of a line camera by means of small auxiliary frame sensors, positioned next to the main imaging sensors on the focal plane. These frame sensors are exposed at a high rate and the shift of their images' contents provides information about the motion of the imaging system. It has been shown by Janschek et al. [2001, 2003] that a special optical correlator hardware can determine the shifts (optical flow) within the images of these sensors in real time. Only these image shifts are saved or transmitted. This is vital because the storage or transmission of the entire auxiliary images would be unreasonably expensive, if not impossible. In a post-processing step, the image shifts can be used to correct the distortions in the line image. Especially if high frequency vibrations affect the camera's orientation during image acquisition this approach achieves very good corrections of the images.

In this contribution we present an approach that is inspired by the successful work of Prof. Janscheck and his colleagues, but suggests two basic innovations. First, we aim to use a standard mobile CPU instead of a special optical correlator hardware. In an empirical test we show that our approach allows to operate at very high measurement rates and can deal with the resulting low image quality and high data rates. Second, we present an approach to derive the exterior orientation of any remote sensing system from the determined image shifts. This way we are able to apply the results to arbitrary sensors. Hence, we also allow the auxiliary sensors to be equipped with separate optics.

In Section 2.2 of this article we present our approach to determine the optical flow in sequences of small images aiming both, high computational efficiency and precision. In Section 2.3 it is shown how the orientation changes of the imaging system can be derived from the optical flow and how these results can be offset-corrected with low-rate or small low cost exterior orientation measurement systems. The results of an empirical test of the approach is presented and discussed in Section 2.4 and concluded in Section 2.5.

2.2 Efficient Optical Flow Determination

The auxiliary sensors are positioned on the focal plane of a main camera or behind separate optics in a way that they are oriented in different directions. Due to their

very small size and a long focal distance the image content moves uniformly in the same direction in the entire image. Hence, it is sufficient to determine a mean image shift vector between every pair of consecutive images. To determine it in real time via image cross correlation requires a special hardware. Unless a special interpolation technique can be used to calculate the image shifts with sub-pixel precision (Janschek and Tchernykh [2001]), true sub-pixel based correlation can't be achieved without major modifications. Another disadvantage is that all structures that are present in a pair of images are used to determine their displacement. Linear structures, which are ubiquitous in urban areas, correlate not only at exactly one shift vector, but also at many different shifts along a line. If there are many dominant linear structures in the image, they can widely overtop the correlation values of remaining non-linear structures that correlate unambiguously.

Our approach only uses structures that correlate clearly at one single shift vector. By ignoring all other structures, not only the effects of ambiguity are reduced drastically, but also a large amount of unnecessary computation time is saved. The findings of Tomasi and Kanade [1991], as well as Shi and Tomasi [1994] provide a very useful solution for the selection and tracking of small, appropriate image regions (features) with very high computational efficiency. According to Tomasi et al. for every pixel of the image the eigenvalues of the 2×2 covariance matrix of image gradients within its 3×3 neighborhood are calculated. A large value of the smaller of the two eigenvalues indicates that the pixel lies on a corner that can be tracked precisely through a series of images. In contrary, if the pixel lies on an improper linear edge or homogeneous area, its smaller eigenvalue is relatively small. Hence, a reasonable number of corners can be selected as trackable features (see Fig. 2.1a and 2.1b). Because the selection of new features requires a relatively large computational effort, it is not performed at every image, but in periodic intervals.

The selected features are tracked with sub-pixel precision through subsequent images using the pyramidal implementation of the Lucas-Kanade Feature Tracker, presented by Bouguet [2000]. Mainly due to image noise, but also for numerical reasons small errors in tracking a feature from one image to another cannot be avoided. This error accumulates while a feature is tracked through a series of images. I causes the feature to drift away from the originally selected corner and unambiguous tracking can't be ensured anymore. To avoid this problem, we track a feature only through a small number of images and then replace it by a newly selected feature. Additionally, we compensate the remaining feature drift in a very efficient way. Every feature is tracked from its position p_1 in the first image of a small series of N images to the last image in two different ways (see Fig. 2.1c). First, a feature is tracked sequentially through all images of the series to the position p_N. Then it is tracked directly from the first image to the position q_N in last image. While the determined position p_N is affected by the errors of $N-1$ tracking steps, the error of the directly tracked position q_N is relatively small. By assuming a linear feature drift, q_N can not only be used to correct the final position p_N, but also the positions p_2 ... p_{N-1} in the intermediate images of the series proportionally.

As p_N is expected to be close to the feature's true position in the last image it can be used support the direct tracking step by predicting the position. This makes the direct tracking step more robust and limits the additional computational effort for the feature

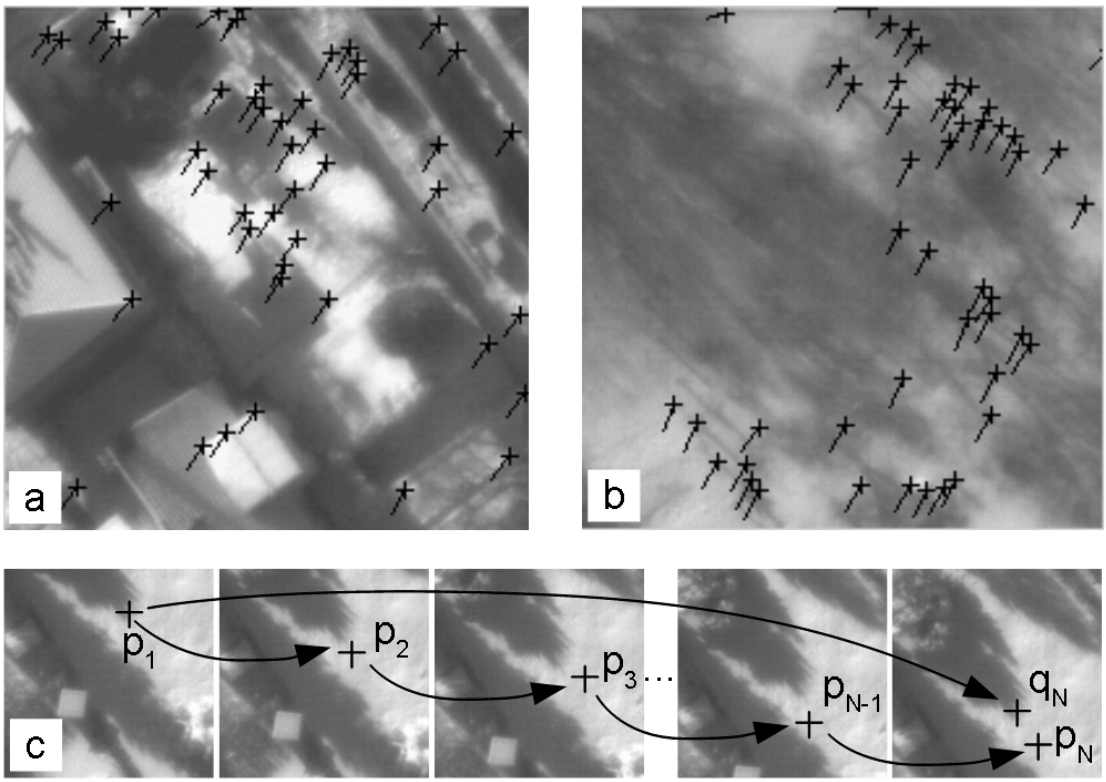

Figure 2.1: Selected and tracked features from the left (a) and right (b) auxiliary sensor (the trail of the features indicates their shift vectors relative to their position in the previous image). The image series (c) illustrates the technique of feature drift compensation

drift compensation to the effort of one regular tracking step each $N - 1$ images.

Incorrectly and inaccurately tracked features are identified by means of basic statistics. From the two-dimensional shift vectors of all features tracked from one image to another the mean value and the standard deviation is calculated. The features with shifts that diverge more than one standard deviation from the mean value are treated as outliers and excluded from further use. The shift vector of two subsequent images is finally defined to be the mean shift vector of the remaining features. By averaging the feature shift vectors, the tracking errors are reduced. The mean shift vector is finally stored or transmitted with the data of the main sensor.

In the following we explain how the orientation of the whole remote sensing system can be derived from the mean image shifts of the different auxiliary sensors, regardless of the approach that was used to determine them.

2.3 Orientation Derivation

The shifts in the images of the auxiliary sensors are caused by both, translation and rotation of the remote sensing system they belong to. As the translation of the camera is assumed to be measured with sufficient accuracy the only unknown variable is the exact orientation of the system. Nevertheless, the orientation is known to be roughly looking down in nadir direction.

Actually also the height of the terrain affects the shifts in the images. The closer objects are to the camera the faster their projections are shifted over the focal plane while it is being translated. Strictly speaking, the optical flow isn't homogeneous if the terrain isn't completely flat. But thanks to the very small base line between two consecutive images and the large distance of the camera from the ground, small elevations (like houses, trees, etc.) don't have a significant effect on the optical flow. This allows the use of a horizontal plane T at mean terrain height as an adequate approximation for the real ground surface. Deviations of the terrain from T in the range of the altitude above ground (e.g. if flying low over mountains and valleys) may result in systematic errors in the orientation. The compensation of these errors is performed in a later processing step.

The presented approach supports a number of two or more auxiliary sensors. In the following we suppose to have the minimal number of two sensors, one directed to the left and one to the right. For both sensors the mean image shift vectors s_L and s_R are available. The difference in spacial rotation δR of the remote sensing system between the acquisition of two subsequent auxiliary image pairs $[I_{L0}, I_{R0}]$ and $[I_{L1}, I_{R1}]$ can be calculated as follows (see also Fig. 2.2). The center of projection O_0 of the first image pair is known. It is assumed that the system is oriented perfectly in nadir direction. The locations of the object points P_L and P_R can be calculated by projecting the central image points p_{L0} and p_{R0} onto the horizontal plane T at mean terrain height. From the mean shift vectors s_L and s_R it is known that the central image points p_{L0} and p_{R0} have been shifted to the points p_{L1} and p_{R1} in the second image pair. As O_1 can be derived from the flight trajectory, δR can be determined by finding the parameters of the rotation (for example three Euler angles) that best satisfy the collinearity constraints with respect to their projections p_{L1} and p_{R1}. This optimization problem can be solved by a non-linear least squares algorithm. For practical reasons we used the the Levenberg-Marquardt algorithm from the sparse bundle adjustment implementation of Lourakis and Argyros [2004], but a basic Gauss-Newton approach is expected to give appropriate results, too.

The absolute orientation of the system can be determined by integrating the differences in rotation over time. Of course, the resulting orientation is biased by a rotational offset R_0. This is caused by the difference between the assumed and the real orientation of the system at the beginning of the integration. Additionally, significant deviations from the assumed mean terrain height cause the orientation to drift away over time. This drift rate can be modeled adequately by a linear drift rate δR_d. The errors of the calculated shift vectors cause a non-systematic drift, which can only approximately be compensated by the linear drift rate. They are the reason for the remaining errors in orientation calculation.

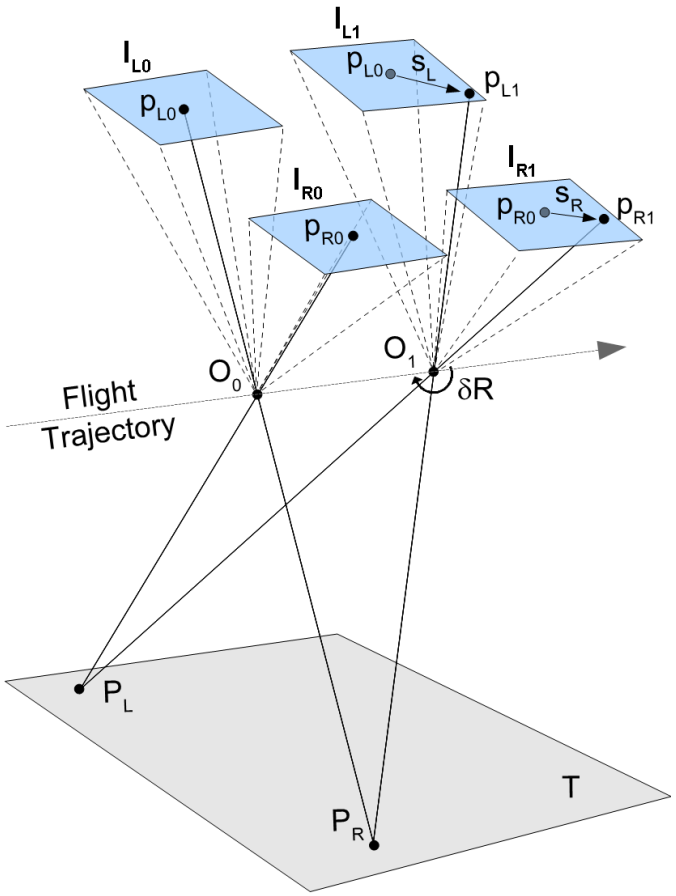

Figure 2.2: Illustration of the orientation calculation from the mean image shifts s_L and s_R in case of two auxiliary sensors positioned behind one single optics with the center of projection O (Not true to scale).

Depending on the type of the remote sensing system and its absolute orientation measurement technique, the rotational offset can be determined in different ways. Remote sensing satellites typically have a very precise attitude and orbit control system (AOCS) with a relatively low measurement rate. The dynamics of a satellite during necessary movements of gyroscopic actuators, solar panels, antennas, etc. is much higher and can be detected well with the auxiliary imaging sensors. In such cases R_0 and δR_d can be calculated for each time interval between two AOCS measurements separately.

The exterior orientation measurement systems that are used in airborne systems typically consist of an inertial measurement unit (IMU) combined with a differential GPS receiver. For such systems, the bandwidth and the measurement noise of the IMU are the main limiting factors for its effective angular and temporal resolution. By averaging the orientation measurements over a floating time interval the measurement noise can

be reduced. By averaging the optically determined orientation over the same interval R_0 can be obtained from the difference of these two averaged orientations. This way, the absolute orientation is provided by the IMU (which is, in turn, stabilized by the GPS and/or a global bundle adjustment, as shown by Wohlfeil and Bucher [2009]), whereas fast orientation changes are determined by the auxiliary sensors. The test results for these two variants are presented in the following Section.

2.4 Empirical Test and Discussion

The presented approach was tested at a test flight over Berlin-Adlershof with the DLR's three-line MFC3-8K camera (Börner et al. [2008]) as main imaging sensor using line-rate of about 435 Hz. Two Prosilica GC640 cameras were used as auxiliary sensors, each equipped with a 100 mm optics that was laterally rotated by 20° (see Fig. 2.3). Each camera captured the central 200 × 200 pixels of its panchromatic CMOS sensor with a frame rate of 480 Hz. Although the extraction of the image shifts is meant to be performed online in a later state of development, at this first test flight all the camera images where recorded and processed offline. The ground sampling distances of the MFC and the auxiliary cameras were similar to allow the determination of orientation changes with an appropriate accuracy for the correction of the line images.

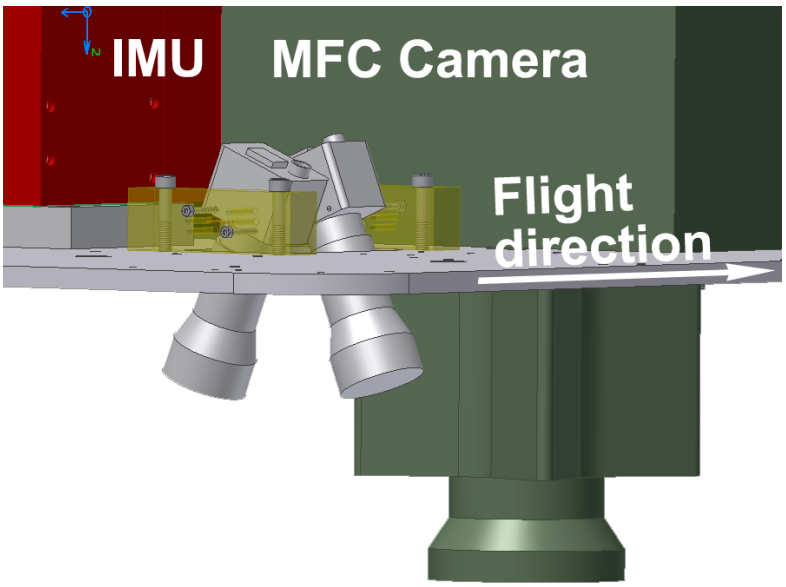

Figure 2.3: Test flight configuration with the MFC camera, the IMU of the IGI AEROcontrol system and the two auxiliary high-speed cameras mounted on the ground plate

To provide a reference measurement, a high-end IGI AEROcontrol DGPS/INS System was used with its IMU mounted on the ground plate next to the other cameras. The

IMU has a sampling rate of 256 Hz but its effective bandwidth is known to be lower than half of this. The limit of the temporal resolution of the optically determined orientation is given by the half frame rate of the auxiliary sensors. To obtain an exact reference measurement a stabilization platform had to be used to suppress orientation changes with frequencies over 100 Hz. The existing ground control points were not usable as a reference because they couldn't be selected with an appropriate precision in the range of hundredths of a pixel.

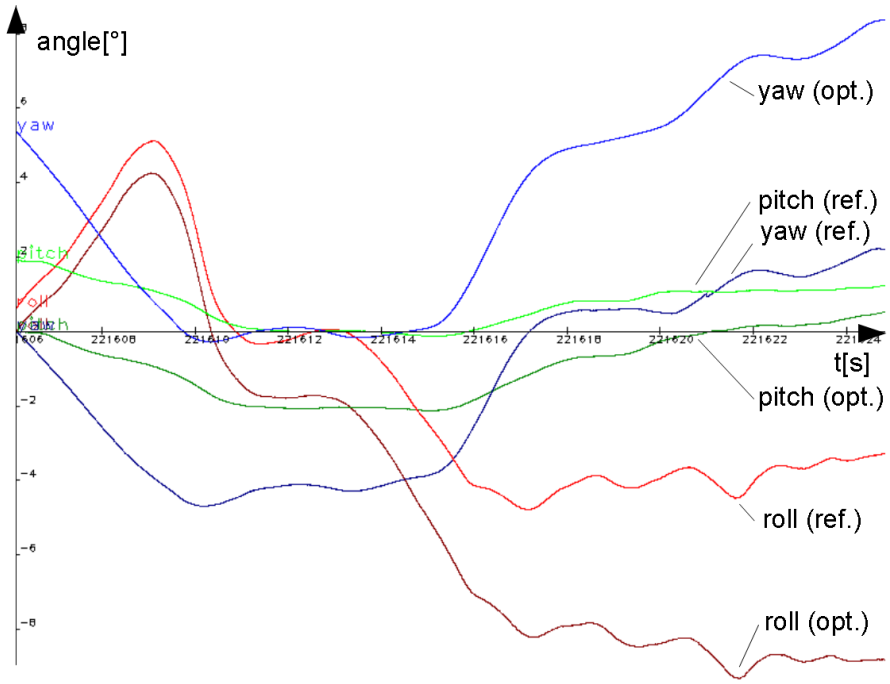

Figure 2.4: Overview of the orientation during the test flight (Euler angles). The reference measurement is illustrated with light lines and the uncorrected optical measurement with dark lines

A line scan with a duration of almost 20 s is used to evaluate different variants of the approach. About 9000 images were captured by each auxiliary sensor during this time. Due to the very short exposure time, the quality of the auxiliary images is poor. Although a pixel response non uniformity (PRNU) correction is performed, there remains a high amount of uncorrectable image noise. Unfortunately, this noise is highly correlated within the rows and columns of the CMOS sensor, causing challenging conditions for any optical flow detection approach. As we aim to operate with cost-efficient sensors at very high frame rates we want to be able to deal with this.

For the test, the image shifts are determined via feature tracking with drift compensation (FT) and via image cross correlation (CC). For both approaches, the two presented variants of orientation offset correction are performed with exemplary configurations.

For the AOCS variant, the orientation of the reference measurement was used in intervals of 1.0 s and 0.1 s to calculate the offset and drift rate of the orientation. For the IMU variant, the reference orientation measurement was overlaid by white noise with an amplitude of 0.01° (around each of the three axes). For the offset correction an averaging interval of 0.2 s turned out to be a good choice with regard to good noise reduction and adequate drift compensation. The RMS and the maximum of differences between the optically determined orientation and the reference measurement are shown in Table 2.1. For a small part of the test the results are illustrated graphically in Fig. 2.5.

	$\Delta roll\,[°]$	$\Delta pitch\,[°]$	$\Delta yaw\,[°]$
	AOCS variant (1.0 s correction interval)		
FT	0.00405 (0.016)	0.00634 (0.026)	0.0185 (0.074)
CC	0.06680 (0.329)	0.0456 (0.222)	0.0583 (0.267)
	AOCS variant (0.1 s correction interval)		
FT	0.00099 (0.009)	0.00114 (0.014)	0.00285 (0.047)
CC	0.00188 (0.011)	0.0016 (0.010)	0.00384 (0.026)
	IMU variant		
FT	0.00163 (0.015)	0.00176 (0.017)	0.00235 (0.048)
CC	0.00203 (0.011)	0.00203 (0.008)	0.00308 (0.013)

Table 2.1: RMS (and maximum) of the differences between optically determined and offset corrected rotation and the reference measurement (Euler angles)

The results in the upper part of Table 2.1 show that the feature tracking approach gives significantly better results than the cross correlation if the reference measurement interval is one second. Thanks to the feature drift compensation, long-term errors are effectively reduced in the feature tracking approach. If the correction interval is only 0.1 s, the results of both approaches are similar (center of the Table). The RMS remains in a range of a few thousandth degrees, which is a fraction of the MFC's angular resolution of 0.0138°. Hence, its images are expected to be correctable accurately with the determined orientation. Also the IMU variant of orientation offset correction proves to achieve good results for both approaches (lower part of the Table).

The main goal of the presented approach is the correction of the main sensor's images. Thus we finally applied the determined orientation to the images of the installed MFC3-8K line camera and evaluate the results. Fig. 2.6a shows a Section of the uncorrected line images (the scanned lines are simply joined together). The image in Fig. 2.6b was corrected with the noisy IMU measurements mentioned above. They obviously have an insufficient precision to correct it adequately. For the image in Fig. 2.6c the optically determined orientation was used (feature tracking and IMU variant of offset correction). The image corrected with the reference measurement is not illustrated because there are barely visible deviations from the image in Fig. 2.6c. If no orientation offset correction is performed, there remain only marginal perspective distortions due to the small orientation offset of a few degrees.

The implementation of our feature tracking approach was able to process 550 frames per second on a laptop with a mobile Intel Core 2 Quad Q9300 CPU for the two cameras

simultaneously in the offline processing test. Processing included the loading of the images, the PRNU correction, the determination of the mean image shift and the saving of the resulting shift vector. As exactly these processing steps are necessary for online processing (except that the images are gathered directly from the auxiliary sensors) this is seen as a proof of the online processing capability of the approach.

2.5 Conclusions and Outlook

The results of the empirical test have shown that the optical measurement of fast orientation changes can be performed with standard hardware which can be characterized by low costs, low weight, and low power consumption. Our approach achieved an excellent accuracy under challenging conditions in the airborne case. We could show that it is possible to determine the orientation with a rate of 480 Hz in real time. This allows many new applications for cost-efficient and high-resolution line cameras and laser scanners; for example their installation in small, unmanned aircrafts.

The results give reason to suggest that the presented approach is applicable to remote sensing satellites as well. Very small orientation changes at fractions of the angular resolution of the main sensor could be determined with a very high rate. Additionally, the influence of deviations from the mean terrain height become negligible because of the very large distance from the ground compared to the height deviations.

Especially because of its high measurement rate and precision, the approach can also be used to evaluate exterior orientation measurement systems with regard to the measurement of fast orientation changes. We plan to perform corresponding tests for different INS/GPS systems.

In the empirical test, white noise has been added to the orientation measurement of a high-end INS/GPS system to simulate a small low cost system. This simulation ignores the reduced long-term stability of low cost systems which causes the orientation to drift away faster and in a higher degree. Such drifts can't be compensated by our approach but it allows to perform an initial correction of heavy short-term image distortions in case of a line camera as main imaging sensor. In the pre-corrected images, well-defined tie points can be selected automatically and be used to correct long-term orientation errors via global bundle adjustment, which will be the subject of further investigation.

As water typically doesn't have trackable structures it isn't possible to detect the image shifts for an auxiliary sensor which is entirely capturing images of a water surface. The image shifts of one single sensor aren't enough to determine the orientation. When only two sensors are used it is very likely that this situation occurs. To overcome this problem we propose the use of three or four auxiliary sensors oriented to different directions. Using this configuration it is very unlikely that three of them are directed towards water, except when scanning a large lake or the ocean. As an additional advantage we expect to gain accuracy due to the additional redundancy in optical flow determination.

The presented technique of feature drift compensation could also be used for the correlation based approach. Instead of correcting the shift vectors of single features, the mean shift vectors could be corrected in a similar manner.

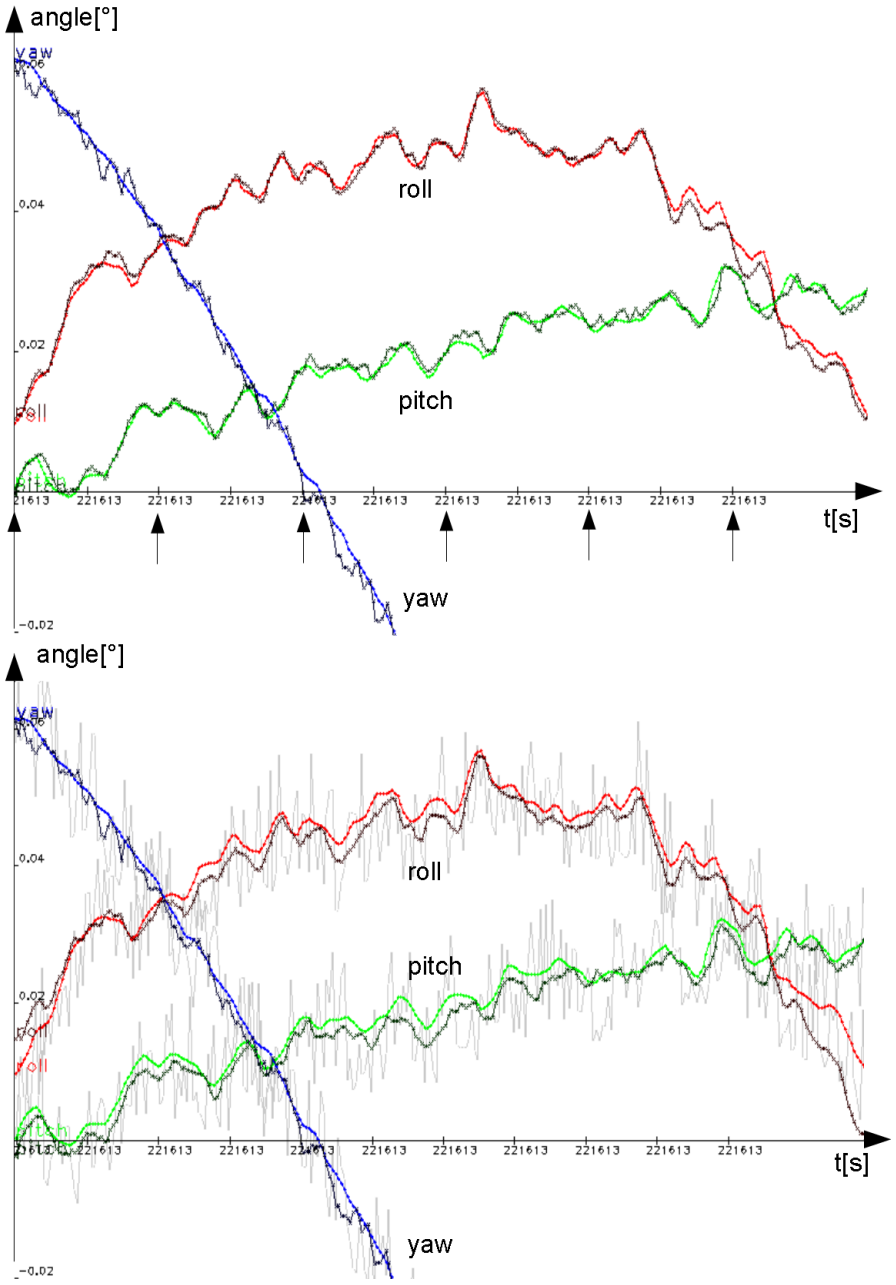

Figure 2.5: A detailed view of the reference measurement (light) and offset-corrected optical measurement (dark) with the AOCS (upper graph) and IMU correction variant (lower graph). The vertical arrows indicate the AOCS correction intervals. The simulated noisy IMU measurements used for the offset correction are drawn in light gray.

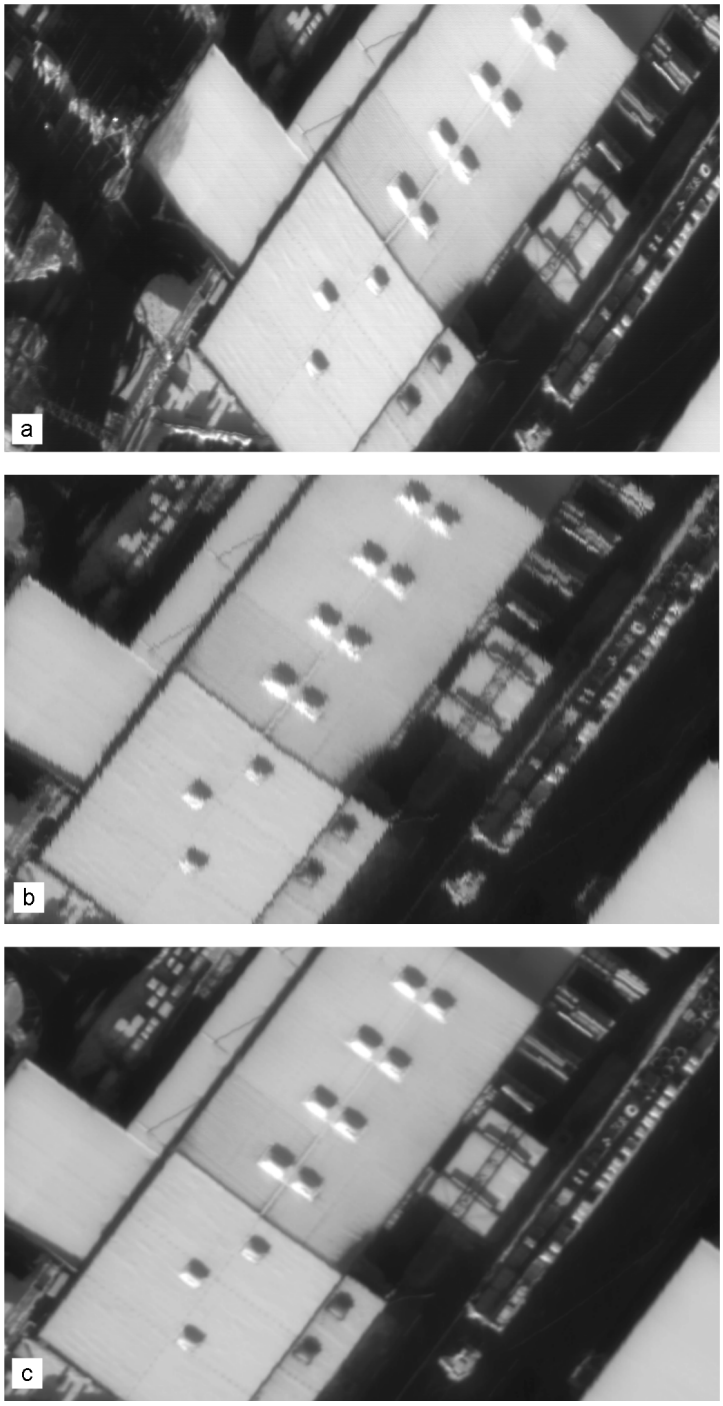

Figure 2.6: The image of the MFC's central line sensor corrected without (a), with the noisy (b) and with the optically determined (c) orientation

Acknowledgments

We want to thank Prof. Beate Meffert from the Department of Computer Science of the Humboldt-Universität zu Berlin for her helpful hints. Also our colleagues from the Department of Sensor Concepts and Application of the Institute of Robotics and Mechatronics of the German Aerospace Center we want to thank for preparing and performing the test flight. Especially Jörg Brauchle for the design and construction of the sensor setup and Dr. Sergey Zuev for the processing of the reference measurement.

3 Completely Optical Orientation Determination for an Unstabilized Aerial Three-Line Camera

Jürgen Wohlfeil

Humboldt-Universität zu Berlin
Department of Computer Science
Rudower Chaussee 25, 12489 Berlin, Germany

German Aerospace Center
Institute of Robotics and Mechatronics
Rutherfordstr. 2, 12489 Berlin, Germany

Abstract

Aerial line cameras allow the fast acquisition of high-resolution images at low costs. Unfortunately the measurement of the camera's orientation with the necessary rate and precision is related with large effort, unless extensive camera stabilization is used. But also stabilization implicates high costs, weight, and power consumption. This contribution shows that it is possible to completely derive the absolute exterior orientation of an unstabilized line camera from its images and global position measurements. The presented approach is based on previous work on the determination of the relative orientation of subsequent lines using optical information from the remote sensing system. The relative orientation is used to pre-correct the line images, in which homologous points can reliably be determined using the SURF operator. Together with the position measurements these points are used to determine the absolute orientation from the relative orientations via bundle adjustment of a block of overlapping line images. The approach was tested at a flight with the DLR's RGB three-line camera MFC. To evaluate the precision of the resulting orientation the measurements of a high-end navigation system and ground control points are used.

3.1 Introduction

Because of the very high line rate and resolution of today's line cameras the measurement of their orientation is challenging. For different applications extensive camera stabilization isn't possible due to limited weight, size or budget. This means that the orientation has to be measured with a very high rate (up to the camera's line rate). High-end navigation systems can achieve this but are very expensive.

Orientation measurement of aerial cameras can be supported a lot by using homologous points (tie points) that can be found in overlapping image regions. When operating aerial frame cameras the orientation measured by the navigation system is often only used as a good initial guess. The precise orientation is determined via bundle adjustment with automatically determined homologous points. One reason why this technique has not been applicable for line cameras for a long time is that line images don't have the rigid geometry of frame images. Basically, every single line of a line image is an independent image with an independent exterior orientation. Another problem is that only lines of different images can be overlapping. To determine the orientation of all lines of overlapping line images a large bundle adjustment with high computational costs is necessary. Also the automatic selection of homologous points in uncorrected, distorted line images is often very unreliable, if not impossible.

Previous work has shown that fast orientation changes of a line camera can be determined using optical information received by the camera system. For any remote sensing system this is possible by using small auxiliary frame sensors with a high frame rate. The optical flow on this frame sensors can be extracted on-line using an optical correlator hardware (Janschek et al. [2001, 2005]) or a mobile CPU (Wohfeil and Börner [2010]). From the optical flow the accurate relative orientation of the remote sensing system can be determined with the auxiliary sensors' frame rate. Only position measurements are needed as additional, non-optical measurements.

For typical multispectral line cameras the relative orientation can be determined using the primary line images (Wohlfeil [2011]), without requiring any additional hardware. It is applicable for cameras that have a set of band-limited sensors positioned in parallel on the focal plane. Each of those sensors has a slightly different angle of view due to its small displacement on the focal plane. Between the images of these narrow sensors homologous points can be detected even in heavily distorted images. With their help the relative orientation of subsequent lines can be determined accurately as well.

The optically determined relative orientation is integrated over time, biased by an unknown rotational offset. Because small errors in the relative orientation sum up over time, this offset is drifting slowly. But in spite of these long-term errors the integrated relative orientation allows to correct the short-term distortions of line images adequately. In these pre-corrected images the automatic selection of homologous points between overlapping line images is by far more reliable than in uncorrected images. The detected homologous points are used to compensate the drifting offsets of the integrated relative orientation via bundle adjustment. This way the absolute orientation of every line can precisely be determined.

In Section 3.2 it is explained how the line images are pre-corrected to enable the

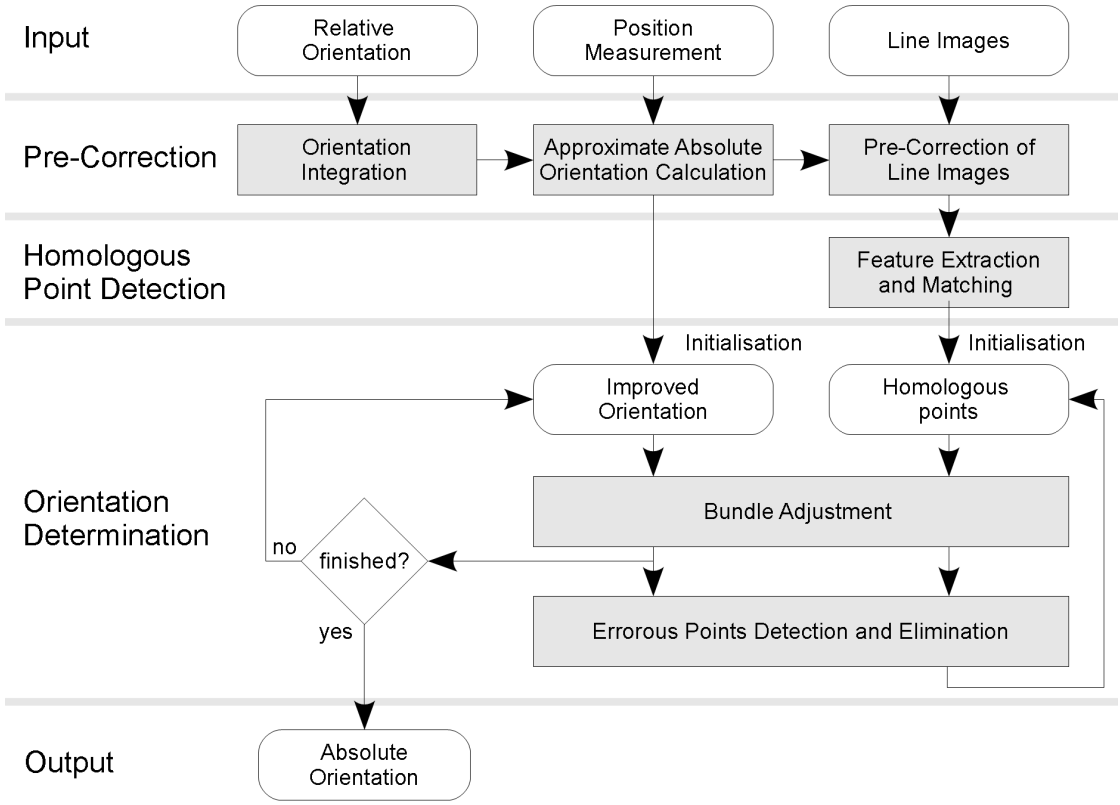

Figure 3.1: The necessary processing steps for the determination of the absolute orientation

automatic extraction of homologous points, as described in Section 3.3. Section 3.4 shows how a whole block of line images can be oriented simultaneously via bundle adjustment. The approach is evaluated at a test flight with the DLR's RGB three-line camera MFC, which is presented in Section 3.5 and discussed in Section 3.6. An overview about the different processing steps is given in Fig. 3.1.

3.2 Pre-Correction of Line Images

To enable the selection of homologous points the line images are pre-corrected by using the optically determined orientation. To achieve this, the yet unknown rotational offsets of the integrated relative orientation are estimated using the position measurements and the nominal camera orientation.

In the long term, the mean roll and pitch angle of the camera is assumed to almost correspond to the camera's nominal roll and pitch angle. The yaw angle can be estimated from the position measurements by assuming that the aircraft is moving roughly in the

direction it is heading for. These three angles define the nominal orientation of the camera, whereas only the yaw angle changes over time.

The nominal absolute orientation and the integrated relative orientation are both averaged over a floating time interval. The difference between these averages is subtracted from the integrated relative orientation, resulting in the approximate absolute orientation. Together with the position measurements this orientation is used to project all lines of a line image onto a virtual planar surface at mean terrain height. On the basis of the resulting pre-corrected images homologous points are selected in overlapping image areas.

3.3 Homologous Point Detection

For the automatic selection of homologous points there exists a large variety of different approaches. The pre-corrected images have two characteristics, from which the requirements for the matching technique are derived. First, corresponding points can be located in different places in different pre-corrected images. This is due to the rough initial estimate of the images' orientation and the possibly large deviations of the actual terrain height from the virtual planar projection surface. Second, errors of the estimated orientation lead to long-term distortions of the pre-corrected images, including rotation, shearing and scaling.

These requirements are met by the technique of matching scale invariant feature descriptors, such as SIFT (Lowe [2004]), SURF (Bay et al. [2008]), and many other variants. In this work the SURF descriptor is used but it is expected that any similar feature descriptor would also be applicable. SURF descriptors are extracted for appropriate image features of every pre-corrected image. They are then compared to the feature descriptors of the other images to find the corresponding features.

A SURF feature descriptor consists of a 64-dimensional vector. Also an orientation angle is determined for every feature. As suggested by the authors of SURF the difference of two features is determined via the Eucledian distance of their descriptors. To reduce the risk of mismatches, features with very different orientations are not considered to correspond because the pre-corrected images are already roughly oriented. Also the possible spacial distance of corresponding features is limited to a reasonable value. This reduces not only the risk of mismatches but also the computational costs for the search of corresponding features.

Let f_i be a feature of an image I_1 and f_j be a feature of another image I_2. Unfortunately their difference $d(f_i, f_j)$ is not a reliable indicator for their correspondence. Much more significant is the ratio of the difference $d(f_i, f_j)$ with respect to the minimum difference between f_i and any other candidate. The correspondence of f_i to f_j can be written as

$$m(f_i, f_j) = \frac{min(d(f_i, f_x))}{d(f_i, f_j)}, f_x \in F_2$$

while F_2 are the features in image I_2 within the spacial search area around f_i, excluding

f_j.

According to this definition $m(f_i, f_j)$ does not necessarily equal $m(f_j, f_i)$. A pair of features is therefore defined to match if $m(f_i, f_j) \geq m_{match}$ and $m(f_j, f_i) \geq m_{match}$. In all possible combinations of overlapping image regions pairs of features are searched. By adjusting the value of the threshold m_{match} the number of resulting pairs of features can be limited to a reasonable amount.

Beginning with the best matching pairs of features, they are extended to N-tuples of features in image areas where $N > 2$ images overlap. In every additional overlapping image $I_n, n \in [2..N]$ the feature f_k is searched that best corresponds to both of the initial pair of features f_i and f_j. If f_k matches both it is added to the existing tuple. Else the whole tuple is entirely omitted. After a tuple of features is complete, all of its members are marked as assigned. Assigned features are not considered to be member of any other tuple during further searches. The positions of the features of every resulting tuple represent one homologous point that is used to determine the absolute orientation of the line images.

Due to specular reflections, moving objects, repetitive patterns, and many more reasons matching errors occur that cause incorrect homologous points. They can have very far incorrect displacements that must be detected and eliminated before the orientation determination can be performed. The most salient and serious errors can be detected by using a very simple consistency check of the displacements. It is based on the assumption that the positions of nearby homologous points are displaced similarly between the same pair of overlapping images. Following this assumption, a homologous point is eliminated if its displacement diverges more than three standard deviations from the mean displacement of nearby homologous points. It is eliminated even if this is true in only one of all possible pairs of overlapping images. This way most of the seriously wrong matched features can be eliminated. Remaining incorrect homologous points are detected and discarded during the iterative adjustment of the line images, as described in the following Section.

3.4 Orientation Determination

The position of the camera is measured via global navigation satellite system (GNSS). For the time periods between the measurements the position is interpolated via cubic spline interpolation. It is supposed that the resulting camera trajectory doesn't diverge from the real trajectory by a relevant amount. The divergence is regarded to be irrelevant if its effect on the image can't be distinguished from an equivalent change in rotation. This applies to most remote sensing cameras due to their long focal distance but has to be verified for a specific system. At the empirical test (presented in Section 3.5) the maximum deviation from the reference measurement (differential GPS, once per second) were 1.2 cm horizontally and 3.3 cm vertically. This is even lower than the typical positioning error of differential GPS and known to be irrelevant for the resulting geometrical accuracy when compensated by equivalent rotations.

Unlike the camera's position, its orientation is completely determined optically. As

explained in Section 3.2 the approximate absolute orientation is biased by a rotational offset that drifts slowly over time. These drifts are modeled by an orientation correction function $C_M(t)$, transforming the approximate absolute orientation $R_a(t)$ into the corrected absolute orientation $R_c(t)$ with

$$R_c(t) = R_a(t) \bullet C_M(t)$$

The operator $\bullet$ represents the addition of spacial rotations via multiplication of unit quaternions. For each scanning period an independent orientation correction function is defined that is able to correct the exterior orientation of one entire line image. If the camera scans more than one line image at once the corrected exterior orientation applies to all of these line images.

An orientation correction function consists of L correction parameter sets, defined for equidistant points in time. Each of these correction parameter sets consists of a unit quaternion, defining a spacial rotation. In order to provide a continuous correction function the quaternion's parameters are interpolated over time via quadratic Bezier curves. The temporal distance between the correction parameter sets Δl is chosen according to the drift characteristics of the optically determined orientation.

Similar to the adjustment of frame images, the appropriate orientation correction parameters have to be found with the help of homologous points. While the correction of a frame image's orientation is typically expressed by a single spacial rotation, the orientation correction function of a pre-corrected line image is more complex and has more correction parameters. In both cases the correction parameters have to be found that meet best the collinearity constraints for all homologous points. To achieve this, a bundle adjustment is performed with $3L$ variable orientation parameters (Euler angles) for each line image and 3 variable parameters for the position of each homologous point. The C implementation of sparse bundle adjustment from Lourakis and Argyros [2004] was used to perform this task.

Due to errors in the automatically determined homologous points, bundle adjustment must be performed repeated in order to detect and eliminate incorrect points. Starting with a correction function of low complexity (large Δl) the most incorrect homologous points can be detected after the first bundle adjustment. They are detected due to their residuals that are significantly larger than the RMS of all points' residuals. After eliminating the detected incorrect points, the complexity of the model is increased by reducing Δl. After performing another bundle adjustment to determine the parameters of this model, some of the remaining incorrect homologous points are found. This procedure is repeated until the necessary complexity of the model has been reached. During this process all incorrect points should have been eliminated, but as few correct points as necessary. A threshold of 3 times the RMS of the current residuals turned out to be a good choice in the experiment, presented in the following Section.

3.5 Empirical Test and Results

The approach was tested on the basis of a test flight with the DLR's 'MFC3-8K' camera Börner et al. [2008]. This camera has three sets of line sensors (12° forward, nadir and 12° backward). Each set consists of a red, a green, and a blue line sensor with an angular offset of 0.077°. At the test flight the camera was directly mounted on the floor of the aircraft without being stabilized at all. As a result the orientation of the camera is directly affected by the vibrations and motions of the aircraft, a Cessna 207. A major component of the high-frequent vibrations was caused by the engine. It is clearly visible in the small vibrations in the uncorrected line image in Fig. 3.2a. Also turbulences caused noticeable and non-systematic orientation changes.

The test flight was performed in Berlin-Adlershof on September 6th in 2007. An area of about 18 km^2 was scanned from an altitude around 950 m with a line rate of 370 lines/s and a ground sampling distance of 12.5 cm in flight direction. The camera's exterior orientation was measured with an IGI AEROcontrol high-end GPS/INS navigation system as reference measurement. In Fig. 3.3 an overview of all scanned images is illustrated. Due to hardware problems that caused gaps and synchronization errors in the line images, some parts of the originally scanned images could not be used for this test.

For the optical determination of the relative orientation the above-mentioned approach for multispectral line cameras Wohlfeil [2011] was used. For images of the MFC it achieves very good results and doesn't require any additional hardware. To provide a position measurement the positions at every full second were extracted from the reference measurement. They were measured with the navigation system's GPS receiver (Novatel OEM4) and corrected with the data of ground-based reference stations. Any other information about the exterior orientation was only used as reference for the comparison of the results.

The offsets of the approximate absolute orientation change significantly in the range of half a second. These changes are clearly visible in the pre-corrected image in Fig. 3.2b. The iterative orientation determination is started with $\Delta l = 8$ s. At each repeated bundle adjustment it is halved until reaching a value of 0.25 s at the sixth iteration. Beginning with geometrical errors of several tens of meters the relative and absolute accuracy is drastically and reliably improved after every bundle adjustment (see upper part of Table 3.1). The relative and absolute accuracy reached after the final iteration is almost as high as the accuracy achieved using the corrected reference measurement (see lower part of Table 3.1).

The improvement of the absolute and relative orientation achieved with the sixth iteration is very small. Taking into account that a major part of this improvement is caused by the removal of the 101 homologous points with the largest residuals it indicates that the complexity of the model is high enough.

The orientations measured by the high-end navigation system are usually corrected when operating the MFC. This is necessary because the measured orientation has small but relevant long-term rotational offsets that change slowly but noticeably. For its correction the same approach was used as for the correction of the optically determined

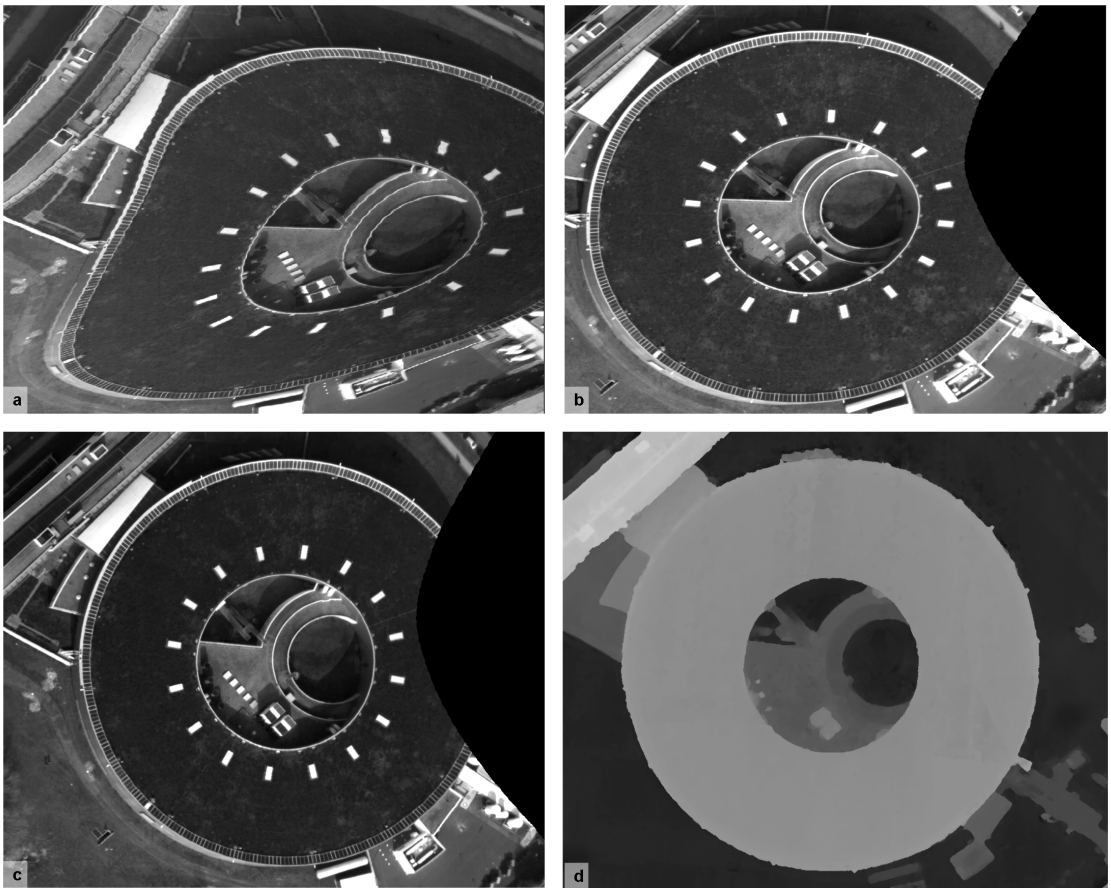

Figure 3.2: **a**: A part of the green band of the uncorrected cross scan (lines are just conjoined). **b**: The same image after pre-correction. **c**: The image completely corrected with the exterior orientation determined by the presented approach (the image corrected with the reference measurement is almost identical and therefore not included in this figure). **d**: A detailed view of the corresponding part of the generated DSM.

orientation. In this case the reference measurement is used as approximate absolute orientation together with the correct homologous points remaining after the sixth iteration. The accuracy achieved with the uncorrected orientation measurement (only sensor misalignment via GCPs) is even lower than the accuracy achieved optically. The absolute accuracy appears to be higher because it is measured at the same GCPs used for the misalignment determination.

A main application of the MFC (and many other line cameras) is the generation of very high resolution digital surface models (DSM) using the semi-global matching (SGM) algorithm of Hirschmüller [2008, 2009]. A very precise epipolar geometry between the line images being matched is vital for SGM. The epipolar curves of arbitrary points must

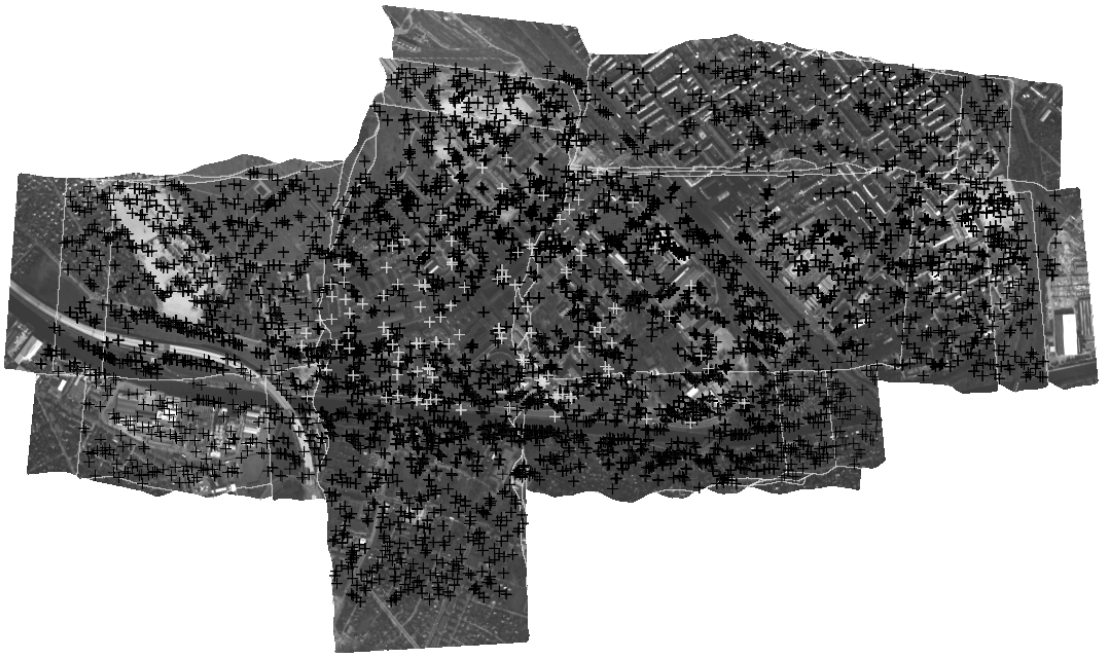

Figure 3.3: Overview of all line images from the test flight projected onto a horizontal plane at mean terrain height. The locations of the ground control points with known positions are marked with white crosses. The automatically determined homologous points are marked with black crosses.

not diverge more than half the DSM's resolution from their true location in order to get reliable and accurate results. An analysis of the divergence of the epipolar curves at the selected homologous points showed an RMS of 7.11 cm. To verify the adequate precision of the epipolar geometry for all pixels in practice, semi-global matching was actually performed on the results.

A DSM with a horizontal resolution of 15 cm could be successfully generated with the optically determined orientation (see Fig. 3.4 and 3.5). There are differences relative to the DSM that was generated using the reference measurements. Most of these differences are caused by matching errors, that occured around water and in partially occluded areas. They are found in both DSMs but have different shapes. From all of the DSM's height values only 9.5 % differ more than 0.5 m and 1.3 % more than 2 m, which is within the range of usual variation.

The time needed to compute the absolute orientation for the presented test flight on an Intel Core i7 CPU with 2.93 GHz consists of the following two parts. About 15 hours were needed to compute the relative orientation from the line images (Wohlfeil [2011]). The processing steps to determine the absolute orientation, as described in this contribution, took about 8 hours. Considering the relatively small area covered by the test flight, the computation time expected for a large area is seriously high. Fortunately

Iter. No.	Δl	**P**ts.	**H**P RMS rel.	**G**CP RMS rel.	**G**CP RMS abs.
initially		4026	34.074 m	41.360 m	54.916 m
1	8 s	4026	6.576 m	5.314 m	50.260 m
2	4 s	3833	0.887 m	1.112 m	4.162 m
3	2 s	3770	0.331 m	0.460 m	0.760 m
4	1 s	3716	0.122 m	0.145 m	0.388 m
5	0.5 s	3663	0.074 m	0.097 m	0.364 m
6	0.25 s	3562	0.062 m	0.095 m	0.358 m
Corr. RM	12 s	3671	0.069 m	0.084 m	0.362 m
Uncor. RM	–	3671	0.111 m	0.138 m	0.283 m

Table 3.1: Upper part: Intermediate accuracy of the repeated bundle adjustment with decreasing Δl and incorrect homologous point elimination. The values in column four are the RMS of the spacial distances of corresponding lines of sight of homologous points (HP). In column five the corresponding errors are listed for the ground control points (GCP). The last column shows the RMS of the distances of the lines of sights from the GCP's absolute positions. Lower part: The corresponding accuracy achieved by using the corrected and uncorrected reference measurement (RM).

there exist some ways to drastically reduce this costs. They are discussed in the next Section.

3.6 Conclusions and Outlook

The empirical test showed that the presented approach is capable of determining the orientation of a line camera with both, a very high absolute and relative geometrical accuracy. To prove its robustness and universality the orientation was completely determined from the line images of the RGB three-line camera MFC. The high computational costs can be justified by saving a high-end navigation system and camera stabilization for hundreds of thousand USD, tens of kilograms of weight, and hundreds of watts of power consumption. The hardware required for the presented results (the MFC and a GPS receiver) could even allow applications with ultralight or even unmanned aircrafts.

The whole processing chain is not yet fully optimized with respect to computational efficiency. Several implementation and algorithm details have the potential to be seeded up a lot. And of course also the continuously increasing processing power of computer hardware supports this approach in the long term.

It is assumed that an additionally installed lightweight low-cost IMU could provide very good initial estimations for the relative orientation of subsequent lines. It is expected that this could drastically reduce the costs for the calculation of the relative orientation. Together with the position measurements a rough absolute orientation could be calculated. It could be used to support the extraction of homologous points and

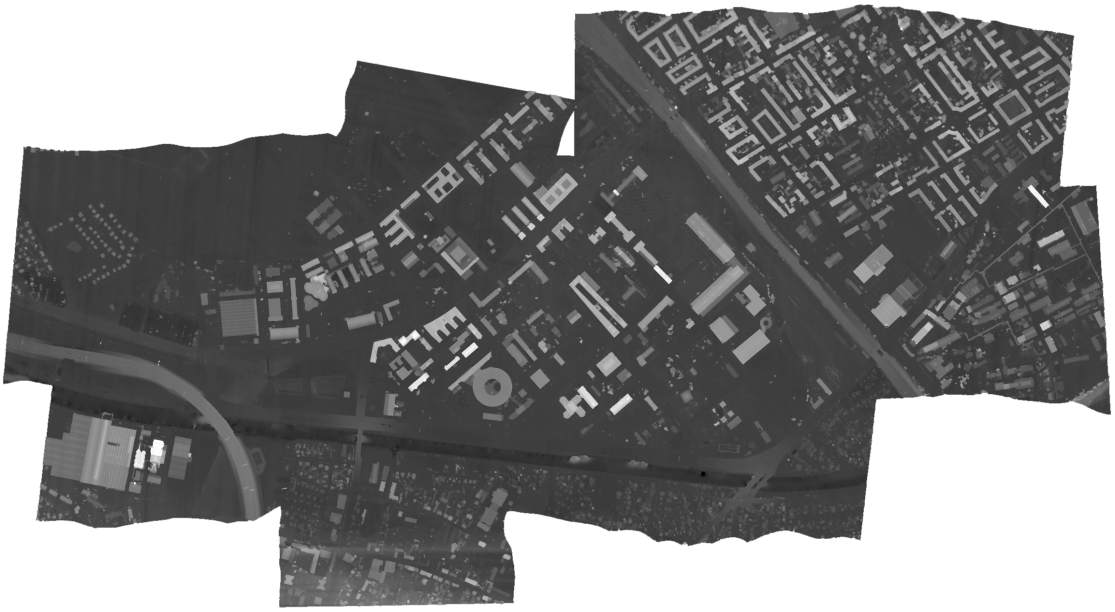

Figure 3.4: The DSM calculated with the optically determined orientation. Dark colors denote a low elevation, light colors a high elevation of the surface. A detailed view a small area is shown in Fig. 3.2.

to provide better initial values for the absolute orientation calculation. This way, even more computational costs could be saved.

The operational application of the approach for large areas is planned to be studied and tested. It offers a solution for enhanced lightweight and low-cost remote sensing systems. Because such systems allow a very economic operation they are very interesting for developing countries and emerging nations. But of course they are also favorable for ecological and environmental reasons.

3.7 Acknowledgements

I want to thank Prof. Beate Meffert from the Department of Computer Science of the Humboldt-Universität zu Berlin for the helpful hints. Also the Department of Sensor Concepts and Application of the Institute of Robotics and Mechatronics of the German Aerospace Center I want to thank for making the test data available for my studies.

Figure 3.5: An oblique view of the generated DSM.

4 Summary

4.1 Results

The main research question of this work was "*How can the orientation of a line camera be measured optically with high angular and temporal resolution and a minimum of technical effort?*". It has been discussed in Section 1.4 why a direct solution is not possible without far reaching restrictions of tolerable types of orientation changes. An answer to the question was found by dividing the main problem into two sub-problems, being solved in two subsequent steps: First, the determination of local orientation changes and, second, the derivation of the absolute orientation.

The two different approaches for the determination of fast orientation changes have been presented in Chapter 2 (frame sensors based approach) and Chapter **??** (line sensor based approach). Both approaches have been tested empirically with real airborne test data. This test data contained urban and rural areas, including moving objects and water surfaces. The results are showing that fast orientation changes are measured with a sufficient accuracy to correct the heavily distorted images. They also show that the approaches work under challenging conditions as well as their particular limitations.

One of the greatest advantages of the line sensor based approach is that it comes along without additional sensors, onboard processing capabilities, or bandwidth. It can be used for existing cameras without modifying them. On the other hand it is only suitable for a particular type of line camera whereas the frame sensors based approach can be applied to any remote sensing system.

When integrating the determined orientation changes small systematic and non-systematic errors sum up and cause the orientation to drift away over time. With the frame sensor based approach lower drifts can be achieved than with the line sensor based approach in comparable situations. The main reason for this is the special feature drift compensation that is possible due to the hundreds by hundreds of pixels wide area of the frame sensors. This technique allows a drastic reduction of non-systematic errors made during the detection of homologous points. But it cannot compensate the systematic errors caused by deviations of the real terrain from the given height value with respect to the altitude of the camera. These effects are only negligible for remote sensing satellites. In the airborne case the deviations can cause high drifts.

In contrast to this, the line sensor based approach estimates the height of every homologous point individually. This avoids the drifts caused by a deviating terrain height. But due to the indirect and loose coupling of lines with a large temporal distance the drift of the determined orientation is generally very high. There are different ways to handle drifts, as shown in all three main Chapters and summarized at the end of this Section.

Other than the wide line sensors each auxiliary frame sensor only observes a small spot of the earth. The empirical tests showed that the determination of the optical flow fails completely if the corresponding sensor is directed onto a water surface. If the optical flow is available for less than two sensors, orientation changes cannot be determined anymore. In contrast to this, the line sensor based approach is much more robust to water surfaces because the full width of the line images is analyzed. Wide water surfaces in the images can be tolerated while extracting the homologous points from the remaining areas of land.

As both approaches describe the determined orientation changes in the same way they are exchangeable. Depending on the application and the sensor configuration the one or the other approach is preferable. The major strengths and limitations of both approaches are listed in Table 4.1.

	Approach based on	
	auxiliary frame sensors	**main line sensors**
Additional onboard hardware	Frame sensors and hardware for online processing	None
Additional bandwidth or storage	Very little	None
Restricted to a particular type of line camera	No	Yes
Size of tolerable water surfaces	Small	Large
Main limiting factor of measurement rate	Frame rate of auxiliary sensors	Line rate of main sensor
Feature drift compensation	Possible	Impossible
Mean terrain height	Must be given	Not necessary

Table 4.1: Comparison of the strengths and limitations of the two presented approaches for the determination of orientation changes.

The second step towards the measurement of the camera's absolute orientation is the determination of the offsets and drifts of the measured orientation changes integrated over time. Different solutions for this step have been presented. In Sections 2.3 and **??** it has been shown that the offsets and drifts can be determined by a conventional orientation measurement system with a low measurement rate or a high measurement noise. This can be an IMU with a low bandwidth and drift in the airborne case or the AOCS of a satellite. With this approach fast orientation changes are effectively measured optically and slow orientation changes with a conventional orientation measurement system.

That the conventional orientation measurement is not even necessary to determine the absolute orientation of an airborne three-line camera is shown in Chapter 3. Beside position measurements this approach only requires the main images and the optically

determined orientation changes to achieve this. For the empirical test the orientation changes were determined with the line sensor based approach. Due to the heavier drifts it is supposed to be the more difficult case and therefore used for testing. An additional motivation for this choice was to demonstrate that a line camera's orientation can be determined only by means of the optical information from its primary images in such a difficult scenario. And in fact a high absolute accuracy of the results could be reached and verified at high-precision ground control points. The achieved accuracy was even high enough to enable semi-global matching being successfully performed on corrected stereo images in the empirical test. These results are very beneficial as this technique allows the generation of high-resolution digital surface models. Not only Gehrke et al. [2010] propose that this is an increasingly important application for stereo line imagery.

4.2 Conclusions

In the three publications, being the main Chapters of this thesis, the potential of optical orientation measurement has been demonstrated with real airborne data. The presented approaches can be used in different combinations and also be used together with other orientation measurement techniques.

A great advantage of the line sensor based approach is that its accuracy increases almost linearly with the angular resolution of the camera. This can be assumed as the accuracy is mainly limited by the precision of homologous points determination in the images. According to this, the achievable accuracy in image space (measured in pixels) is almost the same for line cameras of different angular resolutions. But the achievable angular accuracy (measured in degrees) increases if it is used for a camera with a higher angular resolution. This is a clear advantage compared to other orientation measurement techniques, which have to be improved continuously in order to meet the requirements of new cameras with higher resolutions. Other than this, the presented approach does not need to be modified or improved in order use them for such a new camera.

The measurement rates of both approaches are mainly limited by the frame rate of the auxiliary sensors and the line rate of the camera, respectively. This allows the determination of non-systematic orientation changes with rates up to the camera's line rate. This is very beneficial with respect to all known other approaches targeting optical orientation measurement (except the approach of Janschek et al.). The main limitations of these approaches are given by the simplified models used to describe orientation changes. The reasons for the simplifications are well grounded but are also connected to far-reaching restrictions of the camera's dynamics.

That very fast and non-systematic orientation changes can be measured does not imply that any kind of orientation changes can be tolerated. One limitation of the line sensor based approach concerns the magnitude of orientation changes. As mentioned in Section **??** they must not cause the ground sampling distance to vary by more than $\pm 100\%$.

Another limitation is given by the time needed for the exposure of line and frame sensors. If the orientation of the camera changes very fast and in a high degree the image contents can significantly move over the sensor during its exposure. This can

result in motion blur affecting the extraction of homologous points from the images. Moreover, it cannot be corrected in the line images even if the orientation of the camera is perfectly known. In order to ensure a high quality of the images too drastic orientation changes must be avoided in any case.

The exposure times of line sensors that consist of only one row of photodetectors are usually short enough to prevent a noticeable effect. If Time Delay and Integration (TDI) sensors are used this problem can become more critical. Such sensors consist of multiple lines of photodetectors. According to the speed the image moves over the sensor the charges of the photodetectors are moved from line to line in the sensor. As the electric charges of single photodetectors are accumulated this technique allows integrated exposure times that are longer than the line capturing interval. If the image is not shifted orthogonally and with constant speed over the sensor the quality of the resulting image is reduced. The tolerable frequency and magnitude of orientation changes depend on the total integrated exposure time (Schwarzer et al. [2008]), but also the angular resolution of the camera. If the orientation changes exceed the camera specific limitations passive damping can be used for airborne cameras to reduce the magnitude of the high-frequency vibrations. In contrast to the complete stabilization of the camera this can be achieved with thin and lightweight vibration dampers that may only need to absorb high-frequency vibrations partially.

Although the presented approaches are claimed to be applicable for spaceborne line cameras as well, they were not tested with real spaceborne data. Different spaceborne scenarios have been derived from airborne line imagery, instead. In terms of orientation measurement the most relevant differences between airborne and spaceborne line images is the focal length of the camera and the dynamics of the carrier. Because remote sensing satellites are hundreds of kilometers away from the earth they usually have a very high angular resolution. Due to this, their orientation must be measured with a much higher precision than in the airborne case to achieve an adequate geometrical accuracy of the images.

A remote sensing satellite can control its orientation much more precise than an aircraft can. But due to the much higher angular resolution already very small changes in the satellite's orientation have significant effects on the images. To simulate the spaceborne case data from unstabilized (and incorrectly stabilized) aerial surveys has been used. It is assumed that the resulting fast and heavy motions of the aerial camera have still more serious effects on the images than the motion of a remote sensing satellite. With this assumption the results of the two approaches for the determination of orientation changes are promising with respect to an application for spaceborne cameras.

For the determination of the absolute orientation, as presented for the airborne case in Chapter 3, additional constraints would be necessary for spaceborne applications. Due to the small aperture angle of high resolution sensing satellites the lines of sight, belonging to different pixels of the sensors, are almost parallel. This leads to a very flat error function of the bundle adjustment problem with respect to the absolute orientation. As a result, small errors in the selection of the homologous points have a big influence on the location of the minimum error and so to the solution of the problem. To reliably obtain the precise absolute orientation, ground control points or the direct georeferencing

capabilities of the satellite have to be involved in the bundle adjustment.

The computationally complex steps, including the determination of orientation changes from the line images (Chapter **??**) and the determination of the absolute orientation (Chapter 3) can be performed offline. This is very beneficial as it allows the use of high-performance computers for the complex calculations (Section 3.5). The algorithms used for the determination of homologous points and for the bundle adjustment are suitable for parallelization. Parallel calculation can be implemented within a computer, for example on a GPU (Gupta et al. [2010]) and/or by using multiple computers in parallel (cluster). There are promising prospects to reduce the processing time also by other means, which is subject of future work and described in Section 4.3.

The presented approaches offer the chance to save a large amount of money, weight, and power consumption for camera stabilization and high-end orientation measurement systems in the airborne case. This allows new interesting applications for high-resolution line cameras. One possible application is the use of line cameras on light-weight airplanes with crucial advantages in terms of cost-effectiveness, ecology, and flexibility.

For remote sensing satellites the approaches can help to reduce the idle times needed to let the vibrations of the spacecraft drop below an acceptable magnitude before a scan can be started. By enabling the optical measurement of those vibrations during the scan these idle times can be shortened. This way not only the productivity but also the agility of many existing and future satellites can be improved.

4.3 Future Work

Subject of further investigations are different options to reduce the computational complexity of the above mentioned offline processing steps. Although the implementation used for the presented tests was developed concerning performance issues, there is still a good chance to speed-up the bundle adjustment by a factor of about two or three. An additional speed-up could be achieved by using a lightweight and low-cost IMU that provides good initial values for the bundle adjustment. It can also help to pre-correct the distorted images within the limitations of its bandwidth and measurement noise. By additionally reducing the drift of the optically determined orientation changes a low-cost IMU could also be used to speed-up the absolute orientation determination step. If it has a lower drift than optical orientation measurement it can be used to reduce the number of parameters of the orientation correction functions. As a result, less orientation parameters and less homologous points have to be involved in the bundle adjustment, reducing its computational complexity.

Last but not least the proposed approaches benefit from the continuously increasing computing power of CPUs and GPUs. The implementation and tests on different modern hardware will also be subject of further research.

The operational use of the presented approaches for large aerial surveys with the line camera MFC is planned. Plans also exist to test the line sensor based approach also with images of the aerial line camera ADS. As mentioned in Section 1.1 the staggered sensors of this camera are well suited for the approach and expected to achieve good

results. Also suitable imagery from spaceborne line cameras is hopefully available soon.

In addition to the test with real data more complex simulations are planned to be performed. The simulated data is then used to find out more about the limitations of the approach and its fitness for particular types of line cameras. The ground truth available in simulated data also allows more detailed analyses of the accuracy that can be achieved with the approaches.

In order to avoid oversimplification of the simulated images and camera motion the simulation is intended to be based on real airborne data as far as possible. The simulation on the base of one textured DSM, for example, is known to simplify the images with respect to the detection of homologous points. It neglects at least the effects of moving objects and specular reflections from different viewing angles, being main sources for errors at real data. As a result, the texture of the DSM used to simulate a particular sensor should come from a particular real sensor with a similar viewing angle and spectral sensitivity as the simulated sensor. This implies that the geometry of the real airborne data and the DSM must be very accurate to allow certain conclusions on the accuracy achievable by the different approaches. Although very accurate airborne test data can be retrieved using high-end equipment under optimal conditions the test is planned to be performed with the two types of simulated data: First with the almost realistic simulation with limited precision of the ground truth and then with the precise simulation with simplified conditions for homologous point detection.

Appendix

A.1 Photogrammetrical Concepts and Conventions

A.1.1 Coordinate Systems

Airborne and spaceborne line cameras are used to retrieve optical information about the surface of the earth. Especially the geometrical aspects of this information are important for many applications and subject of this thesis. The global and local coordinate systems are therefore described in detail in this section.

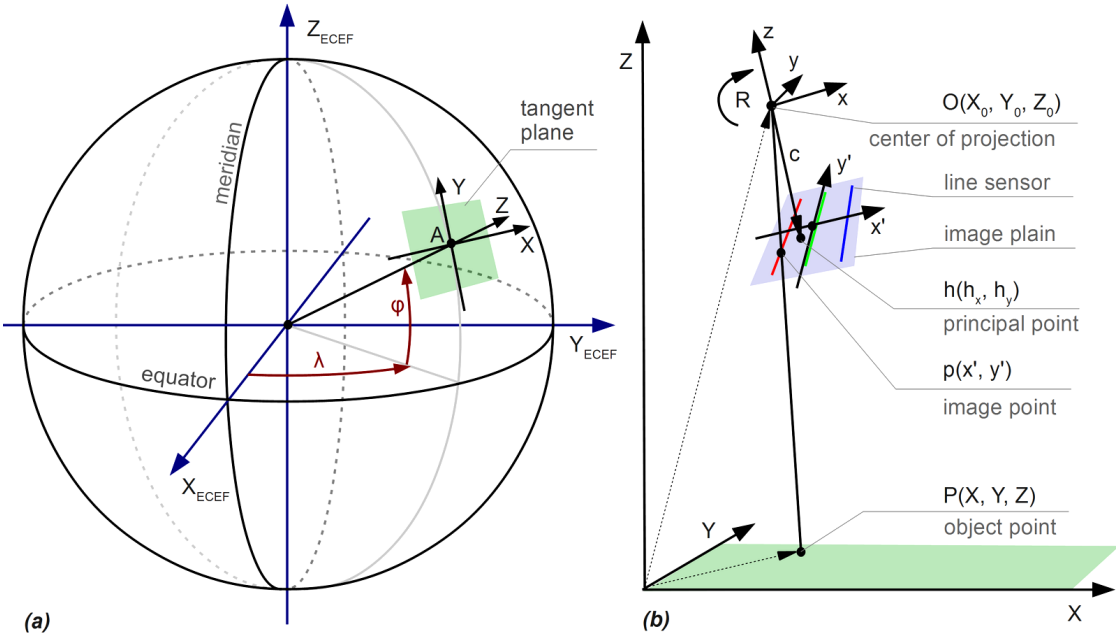

Figure A.1: (a) Relation between geographic coordinate system (longitude λ and latitude φ), earth centered, earth fixed coordinate system (ECEF) and the local rectangular coordinate system (LSR). (b) Projective geometry of a pinhole camera and its coordinate systems. The image plane (also focal plane) is flipped in front of the center of projection

There are several types of coordinate systems used to describe locations on the earth. One of the oldest and still widely used systems is the geographical coordinate system.

It describes the location of any point P on earth by three coordinates: The longitude λ (angular distance from the meridian), the latitude φ (angular distance from the equator) and the elevation specified as the height over the WGS84 ellipsoid (see Fig. A.1a). A great disadvantage of the geographical coordinate system is the matter that it is not a cartesian coordinate system. Geometrical operations which are very simple in a cartesian coordinate system become very complicated in such a spherical coordinate system.

A cartesian coordinate system widely used in spaceborne applications is called "earth centered, earth fixed" (ECEF) or "earth centered and fixed" (ECF) coordinate system. As shown in Fig. A.1a its origin is the center of the earth. The x axis (X_{ECEF}) passes through the intersection of equator and meridian. The y axis (Y_{ECEF}) intersects the equator orthogonal to the x axis, the z axis (Z_{ECEF}) passes through the north pole. This definition implies that the coordinate system rotates together with the earth. It describes the position of any point P on earth by the three cartesian coordinates X_{ECEF}, Y_{ECEF}, and Z_{ECEF} suitable for standard geometrical operations. As the earth has over 6000 kilometers of radius, the coordinates of points on and above its surface have very large values (with respect to relevant distances between object points). This can cause unnecessary numerical issues. In addition to this difficulties, the coordinates of objects on earth are not intuitive in this coordinate system on most regions on earth.

To avoid the above-mentioned difficulties, local space rectangular (LSR) coordinate systems are used (X, Y, and Z in Fig. A.1a). The origin of the coordinate system is a defined point A on earth (in this thesis it is always located on the surface of the WGS84 ellipsoid). The X axis directs to the east, the Y axis to the north and the Z axis away from the center of the earth. The XY plane (tangent plane) is locally parallel to the earth's surface. The LSR coordinate system is rotated by the longitude λ and latitude φ to the ECEF coordinate system and the axes are interchanged. The coordinates of any point can be transformed between these three coordinate systems unambiguously. For these reasons always LSR coordinate systems are used in these theses. The center point A is chosen in the center of the target area.

A.1.2 Geometry of Line Images

The purpose of a camera is to project objects in the three-dimensional object space onto its two-dimensional image plane. This projection can be described as a central projection in the case of the pinhole camera model, where an infinitely small pinhole is the center of projection. The projection of a real camera differs from the pinhole model. These differences, such as lens distortion and other optical aberrations, are described by a camera model. The parameters of this model are called "intrinsic parameters" in terms of computer vision and the "interior orientation" in terms of photogrammetry. In the following it is assumed that a suitable camera model exists and its parameters are known from camera calibration. The corresponding pinhole model with a specific focal length c and principal point $h(h_x, h_y)$ allows geometrical calculations based on the central projection in the pinhole, as described below.

The relation between an image point $p(x', y')$ and the corresponding object point $P(X, Y, Z)$ is given by the central projection and can be described mathematically. There

are two different notations of this relation used in photogrammetry and computer vision. In this work the photogrammetrical notation is used, based on the collinearity equation. For a frame image it is written as

$$\begin{aligned} x'_{ij} &= c \cdot \frac{r_{11} \cdot (X - X_0) \; + \; r_{12} \cdot (Y - Y_0) \; + \; r_{13} \cdot (Z - Z_0)}{r_{31} \cdot (X - X_0) \; + \; r_{32} \cdot (Y - Y_0) \; + \; r_{33} \cdot (Z - Z_0)} + h_x \\ y'_{ij} &= c \cdot \frac{r_{21} \cdot (X - X_0) \; + \; r_{22} \cdot (Y - Y_0) \; + \; r_{23} \cdot (Z - Z_0)}{r_{31} \cdot (X - X_0) \; + \; r_{32} \cdot (Y - Y_0) \; + \; r_{33} \cdot (Z - Z_0)} + h_y \end{aligned} \tag{1}$$

where r_{kl} are the elements of a 3×3 rotation matrix R (equation 4 in Section A.1.3), defining the spatial rotation of the camera coordinate system (x, y, z) with respect to the object coordinate system (X, Y, Z). The translation of the center of projection in the object coordinate system is specified by $O(X_0, Y_0, Z_0)$, as illustrated in Fig. A.1b. The focal length c denotes the distance of the focal plane from the center of projection. The focal plane is intersected by the optical axis z at the point $h(h_x, h_y)$.

The collinearity equation is valid for every pixel at any row i and column j of a frame image. For all pixels the same parameters of the interior orientation $(c, h_x, h_y, ...)$, as well as the same parameters of the exterior orientation (O and R) apply. For line images the same is true, if every single captured line is considered to be an individual image with only one row. If there is more than one line sensor on the focal plane (for example three, as illustrated in Fig. A.1b) which are exposed at the same time, they can be treated as three separate lines of a frame sensor. But as these lines typically have a relatively large distance (in comparison to the distance of subsequent pixels in the line) their image contents cannot be evaluated in a proper way from only one single shot.

In order to get an image of the scene it has to be scanned line by line while the camera is constantly translated (and/or rotated), as illustrated in Fig. 1.1. In other words the exterior orientation is changing while the lines of the image are captured. Regarding the subsequently scanned lines of a line sensor as a continuous image, the indexes of the collinearity equation have to be changed slightly to take this into account:

$$\begin{aligned} {x'}_i^n &= c \cdot \frac{r_{11}^n \cdot (X - X_0^n) \; + \; r_{12}^n \cdot (Y - Y_0^n) \; + \; r_{13}^n \cdot (Z - Z_0^n)}{r_{31}^n \cdot (X - X_0^n) \; + \; r_{32}^n \cdot (Y - Y_0^n) \; + \; r_{33}^n \cdot (Z - Z_0^n)} + h_x \\ {y'}_i^n &= c \cdot \frac{r_{21}^n \cdot (X - X_0^n) \; + \; r_{22}^n \cdot (Y - Y_0^n) \; + \; r_{23}^n \cdot (Z - Z_0^n)}{r_{31}^n \cdot (X - X_0^n) \; + \; r_{32}^n \cdot (Y - Y_0^n) \; + \; r_{33}^n \cdot (Z - Z_0^n)} + h_y \end{aligned} \tag{2}$$

where n denotes the index of one captured line in the sequence, and i is the index of the sensor element (pixel) along the line sensor. The indexes denote that the parameters of the exterior orientation O and R are different for every line of the image. In contrast to this, the interior orientation remains the same for the whole line image. This means that the exterior orientation of a line image with N lines essentially consists of N sets of exterior orientation parameters (O and R).

If the parameters of the interior orientation (c, h_x and h_y) are constant, the collinearity

equation can also be written in a very short form as the function

$$p = \begin{pmatrix} x' \\ y' \end{pmatrix} = f(P,\, O,\, R) \tag{3}$$

where $P = (X_0, Y_0, Z_0)$ and $O = (X, Y, Z)$ are three dimensional vectors and R is a 3×3 rotation matrix as described in the next Section.

A.1.3 Used Representations of Spatial Rotation

Spatial rotation can be described in different ways. The most common definition uses the three Euler angles α, β, and γ (often also called ϕ, ω, and κ, respectively). α describes the rotation around the x-axis, β the rotation around the y-axis and γ the rotation around the z-axis. This way any spatial rotation can be described with three parameters. The resulting spatial rotation depends on the order the rotations are applied and on the decision whether the second and third rotation is applied to the already rotated axes or not. In this thesis the rotations are always applied in the order $\alpha \rightarrow \beta \rightarrow \gamma$ around the original (non-rotated) axes.

Another way to define spatial rotations is the 3×3 rotation matrix. It is characterized as an orthogonal matrix with determinant 1.

$$R = \begin{pmatrix} r_{11} & r_{12} & r_{13} \\ r_{21} & r_{22} & r_{23} \\ r_{31} & r_{32} & r_{33} \end{pmatrix} \tag{4}$$

The relation between Euler angles and the rotation matrix is the following:

$$R = \begin{pmatrix} \cos\beta\cos\gamma & -\cos\alpha\sin\gamma + \sin\alpha\sin\beta\cos\gamma & \sin\alpha\sin\gamma + \cos\alpha\sin\beta\cos\gamma \\ \cos\beta\sin\gamma & \cos\alpha\cos\gamma + \sin\alpha\sin\beta\sin\gamma & -\sin\alpha\cos\gamma + \cos\alpha\sin\beta\sin\gamma \\ -\sin\beta & \sin\alpha\cos\beta & \cos\alpha\cos\beta \end{pmatrix} \tag{5}$$

If the matrix R is multiplied with an three-dimensional vector V, the resulting vector V' is being rotated equivalently to a subsequent rotation by the Euler angles, given in (5):

$$V' = R \cdot V \tag{6}$$

Another representation of spatial rotation used in this thesis is the unit quaternion. It has the great advantage that additions and inversions of rotation can be performed in a very efficient way. There also exist algorithms for the interpolation of rotations represented by quaternions, e.g. SLERP (spherical linear interpolation).

A.1.4 Exterior Orientation

The exterior orientation of a camera describes its position O and the orientation R (Fig. A.1b) at the instant in time when an image is captured. Speaking about the exterior orientation for an image means the exterior orientation of the camera at the moment when the image was captured. The exterior orientation represents the relation between camera coordinate system and object coordinate system and is essential to describe the correspondences between image coordinates and object space. The exterior orientation with respect to the (absolute) object coordinate system is called absolute exterior orientation.

The relative exterior orientation describes the difference between the absolute exterior orientation of two camera poses. Even if the absolute exterior orientation of any of two images is known, the relative exterior orientation describes the relation between points on the two images and points in the three-dimensional object space, relative to the camera positions and orientations. In contrast to this, the position and orientation of these points in the absolute object coordinate system are unknown. But if there are more than two images, whose relative exterior orientation is known, their absolute exterior orientation can be determined if only the absolute exterior orientation of one of these images is known. This can be performed by just adding the relative positions and orientations to the absolute position and orientation of the one image with known absolute exterior orientation.

Let the relative exterior orientation between image I and image J be defined by the translation O_I^J and the rotation R_I^J and the absolute exterior orientation of image I by the translation O_0^I and the rotation R_0^I. By adding the relative exterior orientation between image I and image J to the absolute exterior orientation of image I the absolute exterior orientation (O_0^J and R_0^J) can be calculated in the following way:

$$\begin{aligned} O_0^J &= O_0^I + R_I^J \cdot O_I^J \\ R_0^J &= R_0^I \cdot R_I^J \end{aligned} \tag{7}$$

The rotations R are represented as 3×3 rotation matrices (Section A.1.3) and the positions by 3-dimensional column vectors.

In case of a series of images where the relative exterior orientation between consecutive images is known, the above mentioned relation (7) is of great benefit. If the absolute exterior orientation of one of the images is known, the absolute orientation of all images can be calculated by summing up the relative orientations, image by image. This given relation is one basic element of the division of the main problem of orientation determination into two solvable sub-problems. Regarding every single captured line as a separate image (with only one row of pixels), the relative exterior orientation between all lines belonging to a scanned line image are determined in a first step (Chapter 2 and **??**). Knowing the absolute exterior orientation of only one of the lines, the complex absolute exterior orientation of the whole line image can be derived, which is the principle idea of the approaches for the derivation of the absolute exterior orientation (Chapter 3, but also 2 and **??**). In practice there are small errors in the optically measured relative

orientations between the lines which sum up over time. They cause drifts which have to be determined, too. In contrast to the relative orientations, the relative positions can be measured with very high accuracy via GNSS (e.g. NAVSTAR DGPS).

The known relative positions support the determination of the unknown (or inaccurately known) relative orientations in a high degree. They reduce the number of unknown parameters of the relative exterior orientation between two images from six to three (Euler angles). Moreover, they provide the base distance (distance between the centers of projection) of image pairs, which is indispensable to determine the true scale of object space. This fact is essential for the simultaneous determination of object points and the relative orientation of the camera as used in the approach presented in Chapter **??**, where each captured line is regarded as an image with one line. How this can be performed via bundle adjustment is described in detail in Section A.1.5.

Although the absolute positions of the camera are known via GNSS, the absolute orientation of the camera can only be determined roughly with this approach. This is because the angular difference between the line sensors is required to be very small in order to find corresponding image points reliably. On the other hand, these small angular differences cause the base distance between two line sensors when capturing the same point to be very small (in comparison to the distance of the object point from the camera). Beside of many advantages for determination of corresponding image points (explained in detail in Section **??**), this geometry has the great disadvantage that the absolute position of object points visible in the images can only be determined with low precision. As they are captured from almost the same position, it is not clearly distinguishable in which direction an object point is located relatively to the cameras known absolute position. In turn, this means that the camera's absolute orientation cannot be determined precisely. One way to solve this problem is to increase the base distance of the images being oriented.

In other words: If the base distance between two images, containing the projections of the same object points, is large in comparison to the distance of the object points from the camera, then the absolute position of these points can be determined accurately. This means that also the absolute orientation of the images can be determined with high precision. The presented approach for the determination of the camera's absolute orientation (Chapter **??**) takes advantage of this connection by using images from very different positions. How the camera's absolute orientation can finally be determined via bundle adjustment is explained in the following section.

A.1.5 Bundle Adjustment

In images that (partly of fully) show the same scene, corresponding points can be determined manually or automatically (as explained in Section A.2). Such corresponding points are often called homologous points as their projections (image points) belong to the same location (object point). Homologous points represent geometrical relation between different images. This is why they are sometimes also called tie points. In contrast to ground control points, whose positions in object space are known, the positions of homologous points are initially unknown.

The problem of simultaneously finding the locations of homologous points (P_m) and the exterior orientation (O_n, R_n) of each of a group of overlapping images n is called bundle adjustment problem. The problem is solved by adjusting the exterior orientation of the images in a way that leads to the physically expected intersections of the bundles of light rays at the corresponding object points and centers of projection. If the locations of the homologous points and/or the centers of projections are wrong, the homologous points are predicted to be projected onto wrong image points q_{nm}, due to the wrong input parameters (P_m, O_n, and R_n) for the collinearity equation (3). They are wrong as they differ from the true position of the image points p_{nm} observed in the images.

In other words, there is a difference between the predicted position q_{nm} of the image points and their true position p_{nm}, which are called reprojection errors. These errors are to be minimized by finding the most suitable input parameters. In this way, the bundle adjustment problem can be transferred to the problem of minimizing the sum of the squared Euclidean distances $d(q_{nm}, p_{nm})$ between predicted and observed point positions:

$$\min_{P_m, O_n, R_n} \sum_{n=1}^{N} \sum_{m=1}^{M} d(q_{nm}, p_{nm})^2 \cdot v_{nm} \tag{8}$$

where

$$q_{nm} = f(P_m, O_n, R_n) \tag{9}$$

and

$$v_{nm} = \begin{cases} 1, & \text{if point } m \text{ visible in image } n \\ 0, & \text{else} \end{cases} \tag{10}$$

N is the number of images and M the number of homologous points involved in the bundle adjustment. n is the index of an image and m the index of a homologous point.

If there are initial values available for the sought parameters, the error can be minimized with nonlinear least-squares algorithms like the Gauss-Newton algorithm. Starting with an initial guess of parameters a, the Jacobi matrix J is calculated, consisting of the first-order partial derivatives of the collinearity equation for all observed image points with respect to all sought input parameters a. In each iteration the equation

$$(J^T J)d = J^T r \tag{11}$$

is then solved for d, where r is the vector, consisting of the values of all collinearity equations with the current set of parameters a. The improved parameters a_{i+1} are then calculated by adding the vector d to a_i:

$$a_{i+1} = a_i + d \tag{12}$$

This iteration is repeated until the sum of squared differences between the observed and sought parameters is below a defined threshold or does not change in a relevant

degree between two iterations. The current set of input parameters is then considered to be the best solution of the given bundle adjustment problem.

The vector d can be regarded as the local descending direction of a multidimensional error function at the position, given by the vector a_i. As the descending direction is only locally calculated, it can happen that the algorithm leads to a local minimum error, instead of the global minimum error. The risk to reach a local minimum is highly dependent on the shape of the error function, which is, in turn, dependent on the specific bundle adjustment problem.

The locally determined vector d can lead to a big step in a wrong direction as the local descending direction may vary a lot from the direction towards the global minimum. Such mistakes increase the chance to reach a local minimum even more. As an extension of the Gauss-Newton algorithm, the Levenberg-Marquardt tries to avoid such problems with an additional damping factor, which is adjusted after every iteration. The robustness of the Levenberg-Marquardt algorithm is confirmed in the extensive empirical tests in three very different applications.

In Chapter 2 the orientation of a remote sensing system is measured based on the image shifts in two or more auxiliary frame sensors. The problem of determining the change of the system's orientation between the capture of two pairs of frame images with known image shift is formulated as bundle adjustment problem. Essentially this involves only three unknown parameters, which are the Euler angles describing the change in rotation. The observed image shifts s are used to define one virtually known object point P in each image. As described in Section 2.3 its position is calculated by intersecting the line of sight, belonging to the central pixel, with the ground plane T (illustrated in Fig. 2.2). This is possible by assuming that the remote sensing system is rotated in nadir direction (R_0). The corresponding image points are the central pixels p_{N0} in the earlier image and $p_{N1} = p_{N0} + s$ in the later image captured by the sensor N. This leads to two object points with virtually known positions observed by the two frame sensors in the later image. According to (8), the specific bundle adjustment problem is formulated by

$$\min_{R_1} \left(d(q_{L1}, p_{L1})^2 + d(q_{R1}, p_{R1})^2 \right) \tag{13}$$

and solved for R_1. q_{L1} and q_{R1} denote the locations of the image points according to the short notation of the collinearity equation (3)

$$\begin{aligned} q_{L1} &= f(P_L,\, O_1,\, R_1) \\ q_{R1} &= f(P_R,\, O_1,\, R_1) \end{aligned} \tag{14}$$

and p_{L1} and p_{R1} the locations determined by the image shifts.

Most of the parameters involved in this small equation system are already known. O_0 and O_1 are determined via GNSS. P_L and P_R are estimated by roughly guessing the height of the terrain, and also p_{L1} and p_{R1} have been calculated using the determined image shifts. The three angles of R_1 are determined via bundle adjustment and so δR as the angular difference between R_0 and R_1. As the number of equations is very low,

even if three or four cameras are involved, the solution can be calculated very fast. This is essential as the changes in orientation have to be determined in real time. In the implementation, R_0 and R_1 are represented by Euler angles but other representations like unit quaternions, for example, would be suitable as well.

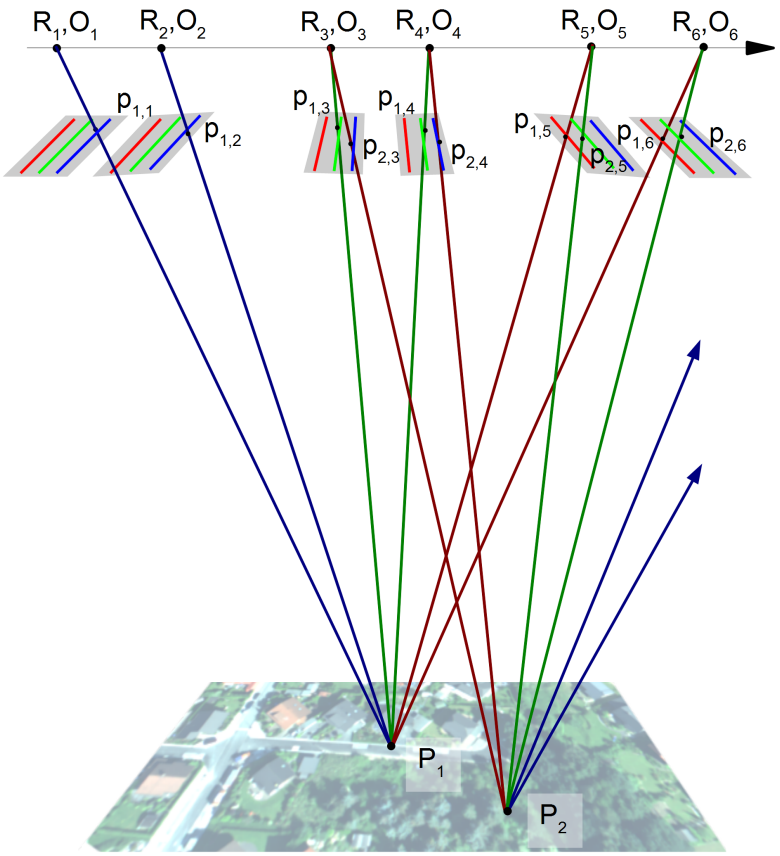

Figure A.2: Visualization of the bundle adjustment problem for multi spectral line images. The figure is not true to scale: The focal distance and the angular differences of the spectral bands are oversized.

In Chapter **??** the orientation of a remote sensing system is measured based on the images of a typical multispectral line sensor. As it is assumed that the camera can have a different orientation at the capture of every line, the corresponding bundle adjustment problem becomes very complex. In addition to Fig. **??** the bundle relation between the camera's orientation and the extracted corresponding image points is illustrated in 3D in Fig. A.2.

The horizontal arrow denotes the movement of the camera over time. The centers of projection at the moments when six different lines were captured are marked with small dots on the arrow. The corresponding camera rotations are illustrated by the rotation

of the grey focal plane with respect to the center of projection. It is shown that the homologous point P_1 is observed three times while it was scanned by a camera with three line sensors. As the lines are captured at discrete times, an object point is defined to be captured two times from each sensor in the lines that were exposed immediately before and after the projection of the point crossed the sensor. This means that there exist a total of six observations of every homologous point using a camera with three line sensors.

Even though the positions of the homologous points are unknown, the fact that they were observed at different points in time helps to determine the orientation of the camera. This is because the homologous points act as links between the orientations of the camera during the scan of the image. For the example given in Fig. A.2, six equations can be written for the first homologous point (P_1) and six more for the second (P_2):

$$\begin{aligned}
p_{11} &= f(P_1, O_1, R_1) \\
p_{12} &= f(P_1, O_2, R_2) \\
p_{13} &= f(P_1, O_3, R_3) \\
p_{14} &= f(P_1, O_4, R_4) \\
p_{15} &= f(P_1, O_5, R_5) \\
p_{16} &= f(P_1, O_6, R_6) \\
\\
p_{21} &= f(P_2, O_3, R_3) \\
p_{22} &= f(P_2, O_4, R_4) \\
p_{23} &= f(P_2, O_5, R_5) \\
p_{24} &= f(P_2, O_6, R_6) \\
p_{25} &= f(P_2, O_7, R_7) \\
p_{26} &= f(P_2, O_8, R_8)
\end{aligned} \tag{15}$$

The upper six equations are related due to the homologous point P_1 and the lower six due to the homologous point P_2. As P_1 has been captured by the green sensor while P_2 was captured by the blue sensor, the camera is known to have the same exterior orientation in both cases. This is why R_3 occurs in both equations and acts as a relation between the upper and the lower group of equations. Obviously this is also true for O_3, but as the positions are known (measured via GNSS) it is treated as a constant. Similarly three more simultaneous observations of the two homologous points with different line sensors interlink the system of equations (due to R_4, R_5, and R_6).

With a growing number of homologous points the network of equations becomes more and more interlinked. As the orientation of every single line has to be determined, a high number of homologous points have to be used to interlink a reasonable number of subsequent lines (sections) of a line image. This results in a very large system of equations that has to be solved in every iteration of the bundle adjustment. To reduce the huge computational effort, that would be necessary for the bundle adjustment, the sparse nature of the Jacobian matrix J is used. Because each of the sought parameters in a only influences very few of the equations in (15), most of the first order derivations

the Jacobian matrix contains are zero. By making use of this fact, the solution of (11) can be speeded up in a very high degree, as shown by Lourakis and Argyros [2004], for example, whose approach is used in this thesis.

A.2 Finding Corresponding Image Contents

A.2.1 Feature Matching

In order to determine the orientation of a line camera via bundle adjustment, homologous points have to be determined in overlapping images. A homologous point (also called "tie points") is a point in object space whose position is initially unknown. Only the corresponding image points of its projection into two or more images are known. Homologous points can be selected manually by marking the position of an object in the images. But there are also ways to perform this task automatically with modern image processing techniques. In this context the term "image features" is used rather than image points as it is almost impossible to determine single corresponding image points reliably. Instead, a small image region around an image point has to be evaluated, containing a salient feature of the image.

The general approach for the automatic selection of corresponding image features can be divided in two steps. In the first step, features are selected in overlapping images that appear to be assignable clearly and unambiguously to the corresponding feature in another image. In a second step, the corresponding (matching) image features are determined. To perform the second step only with the selected features does not only save a lot of computation time for the matching of unsuitable features, but also reduces the chance of mismatches in a high degree.

Image regions with homogenous greyvalues are obviously not suitable for the determination of corresponding image points. More suitable are regions where the greyvalues change in a relevant degree. But even if the greyvalues are very different, there is a variety of problems that make the matching of image features difficult. In Fig. A.3 examples are given to explain some of these problems.

Feature 1 shows a region where the greyvalues change along the road marking, but unfortunately there are plenty of suitable image regions along the road marking in the right image (1a, 1b, 1c and many others). The problem is caused by the fact that linear edges cannot be assigned unambiguously. This is why most image matching approaches only select features where greyvalues change in different directions. Such image features are called corners. In Fig. A.3 feature 2 is such an edge, which can be clearly assigned to the corresponding image region in the right image.

But although feature 3 is clearly a corner, its correspondence in the right image is not clear by only comparing the image regions. Especially in human made environments repetitive patterns occur very often, leading to mismatches. Another problem are discontinuities in the shape of objects, as for example in case of feature 4. From the perspective of the right image, the feature is optically divided into two fragments. Feature 4 may still match feature 4a or 4b, but also a pattern between them, if the shift is not as large as in this example, although basically there does not exist any clearly

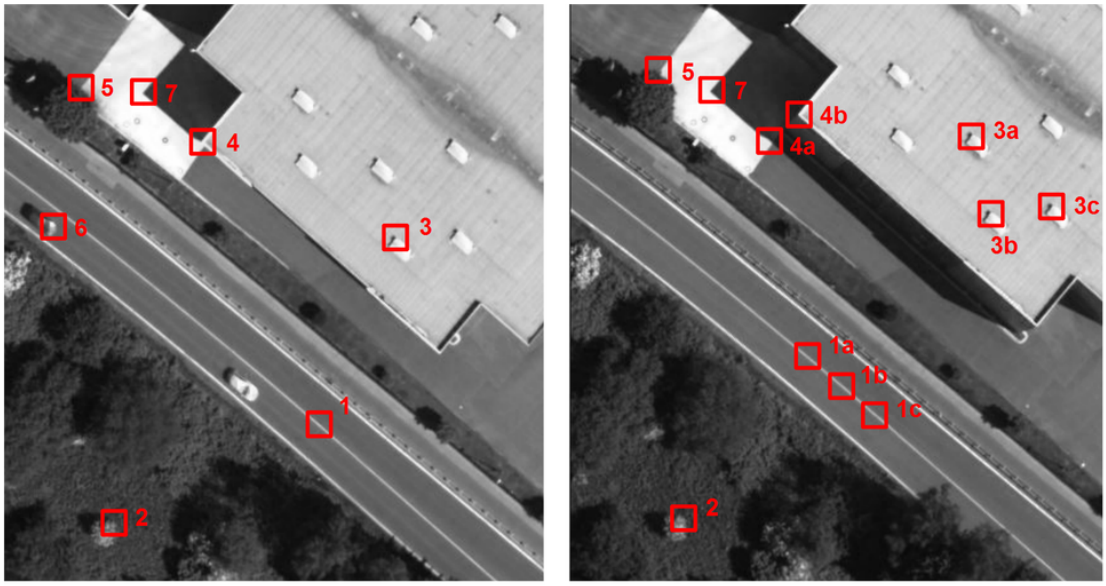

Figure A.3: Example of difficulties in finding corresponding image points in stereo images (approximately 25° stereo angle)

corresponding feature. The same is true for feature 5 in the left image which visually corresponds to feature 5 in the right image. But there is no physical representation of a corresponding homologous point in object space as the feature consists of a visual intersection of lines (the border of the tree and the border of the paving) which do not intersect in object space.

Another problem are objects that move during the time between the capture or the scan of different overlapping images. In Fig. A.3 there are two cars in the left image which are not visible anymore in the right image. In this case there is no correspondence to feature 6, but if the car would have moved only a small distance there would be a clearly corresponding image feature. Although the mach would be correct, it would not correspond to an homologous point as the car has been in different locations in object space when the images were captured.

Also shadows move during the day and can have similar effects as real moving objects because they typically have sharp corners which make them appear like suitable features (e.g. feature 6). It is almost impossible to reliably recognize shadows in a single band in order to exclude their features. Even the reflection of the sun on reflecting surfaces may move while the sun and/or the camera moves. Due to all these problems there are various consistency and plausibility checks included in the approaches, presented in Chapters 2, **??**, and 3. Without these checks the determination of the orientation would not be possible due to too many undiscovered mismatches and in turn to too many wrong assumptions about the relations between the images/lines.

Unfortunately, there is no universal approach to find corresponding image points in

any kind of images taken from any kind of objects. But there exists a variety of different approaches with different advantages and disadvantages. They are briefly described in the following section and the background of the choice of the particular approaches is given.

A.2.2 Approaches

One basic approach for the matching of small image regions is the cross-correlation of greyvalues. The result of the correlation is supposed to be high if the correlated image regions are similar and it is supposed to be low if they have different contents. To reduce the influence of illumination differences on the result of the correlation the normalized cross-correlation (NCC) is used, which norms the greyvalues before correlating them. The matching of features is performed by a search for the displacement of the image region in the second image with the highest correlation with the image region in the first image. Depending on the size of the image regions and the possible displacements the computational effort for such a search can be very high.

A faster approach to the problem was presented by Kanade, Lukas, Tomasi et al. in and around the years 1991 and 1994. It is often named KLT-Tracker after the initials of its main inventors and its most popular application, the tracking of objects through sequences of images. Similar to the previous approach it searches for the displacement where the contents of two image regions correlate best. But instead of evaluating the correlation at every possible displacement, which is very costly, it estimates the displacement by local linearization of the greyvalue gradients. This guess is improved in a small number of iterations until the best match is found. As the linearization of the greyvalues can only approximate the real greyvalues for a very small area, the approach can only determine displacements up to one pixel. At least the displacement is determined with sub-pixel precision. In order to allow the determination of larger displacement, the approach was extended by a pyramidal implementation by Bouguet [2000]. Starting at the top of an image pyramid of downscaled images, very large displacements in the full resolution image can be handled. By iteratively descending the pyramid towards the full resolution the determined displacements can be refined more and more until the actual displacement can be determined with sub-pixel precision.

Both, cross-correlation and KLT-Tracker, work with relatively small image regions but can also be applied to match features of 30×30 pixels or even more. But in large image regions the deformation of the contents due to the different perspective of the images often prevents the determination of the correct match. This is why they best work with features of the size from about 3×3 to 7×7 pixels. Due to the small size of the features the maximum reasonable displacement of the features should also be kept small because for such small features the probability of random matches with non-corresponding image regions is very high.

Another group of feature matchers allows basically any displacement between features of different images by using feature descriptors. These feature descriptors are calculated for small regions around so-called key points which are assumed to be assignable unambiguously to the corresponding regions in another image. For each of two overlapping

	typical effective feature size (image region)	maximum reasonable displacement	displacement determined with sub-pixel precision	invariant to scale, rotation and shearing	invariant to illumination changes	computational effort (relative)
cross-correlation	3 - 7	30			✓(NCC)	very high
KLT-Tracker	3 - 7	30	✓			low
SIFT	8 - 32	∞	✓	✓	✓	high
SURF	9 - 27	∞	✓	✓	✓	high

Table A.2: Comparison of different feature matching approaches suitable for the determination of corresponding image points

images, feature descriptors are calculated and stored in a database. Corresponding features are found by comparing the Euclidean distance between the descriptors of features from different images.

The most popular approaches of this group are SIFT (Scale Invariant Feature Transform, Lowe [2004]) and SURF (Speeded Up Robust Features, Bay et al. [2008]). Both are invariant to scale, rotation, and shearing, which means that their descriptors match even if the features are visible in a different scale, rotation, and shearing in the two images. The main difference between the two approaches is the calculation of the feature descriptor.

SIFT builds up histograms of the orientations of the greyvalues within a small image region which are rotated relative to the main orientation of the feature. Typically 4×4 histograms for the quadrants around the key point are created, each with 8 orientation bins, resulting in a descriptor size of 128 values.

SURF makes use of integral images to convolve the image region around the key point with approximated Gaussian second order partial derivatives in x, y, and xy-direction. The results of the convolutions with different kernel sizes are rotated relative to the main orientation of the feature, stored in a feature descriptor with typically 128 values.

Due to the use of integral images the SURF approach is faster than SIFT and achieves comparable results. But compared to the KLT-Tracker both need a relatively high computational effort. Their huge advantage is that the displacements between the features are basically unlimited. Also in a database with a huge number of features, corresponding features can be determined with relatively high confidence as the feature descriptors contain relevant details of a relatively large image region around the feature. Another important advantage is, of course, the invariance to scale, rotation and shearing.

A.2.3 Choice of the Appropriate Approaches

Different feature matching approaches have been applied in the context of this thesis. The background of the decision for the one or the other approach shall be explained in this section.

In Chapter 2 the shifts of the images of small auxiliary frame sensors have to be determined with sub-pixel precision and minimal computational effort. As explained in Section 2.2 these requirements can only be met if a small number of small image regions are tracked efficiently from image to image. Due to the very high frame rate the displacement of the images' contents is limited to distances up to a few pixels and they are only rotated or scaled in a negligible degree. Table A.2 clearly shows that the KLT-Tracker is the only suitable approach under these boundary conditions.

For the matching of distorted line images of different spectral bands in Chapter **??**, the compensation of the radiometric differences is an essential need. The solution of this problem is described in detail in Section A.2.4. Next, a huge number of features has to be found and matched in very distorted images. Unfortunately the representations of corresponding feature are distorted in different ways in different spectral bands as they are scanned at different instances in time. To reduce the influence of these distortions the size of the features has to be kept as small as possible. At the same time the displacements of the features in different bands are not expected to be larger than a few pixels. These requirements again lead to the KLT-Tracker, which impresses with its great efficiency and sub-pixel accuracy. But even if efficiency would not be a requirement, SIFT and SURF would not be suitable due to the large size of their features and their incapability of tolerating deformations with high frequency.

For the determination of the absolute camera orientation from a block of overlapping line images in Chapter 3, the requirements are different. As the absolute orientation is only guessed very roughly in the initial phase of processing, the displacement between corresponding image points can be very large (up to thousands of pixels). The images are still distorted but the distortions are more global and do not change within tens of pixels in a relevant degree. A look at Table A.2 shows that the approaches which tolerate distortions like scaling, rotation, and shearing and allow large displacement at the same time are SIFT and SURF. For the implementation SURF was chosen due to its slightly better performance but generally both are applicable.

A.2.4 Radiometric Balancing

The approach for optical orientation determination of a multispectral line camera (Chapter **??**) requires several steps of preprocessing until corresponding points can be detected reliably. One important step of those is the radiometric balancing which is only explained briefly in the article. This section gives a more detailed description of the underlying algorithm.

The problem of finding corresponding points in images of different spectral bands is, that object points may appear with very different intensities in different bands. This is because materials typically reflect or emit some parts of the light spectrum in a higher

degree than others. In the lower part of Fig. A.4a there are two houses with a red roof which have high intensity values in the red band and low intensity values in the green and blue band. It is also obvious that green meadows and trees appear brighter in the green band.

The example in Fig. A.4a also shows that the greyvalue changes within the boundaries of an object of the same material are similar in the different bands. By adding a suitable offset to the greyvalues in one band and additionally scaling them with an appropriate scale factor, they can be approximated very well to the greyvalues of another band in many cases. This observation leads to a simple but effective way to make the different image bands more similar and thus more suitable for feature matching. By locally maximizing the greyvalue range, a good offset and scale factor are found for every band that make the greyvalues similar in a small region of the image.

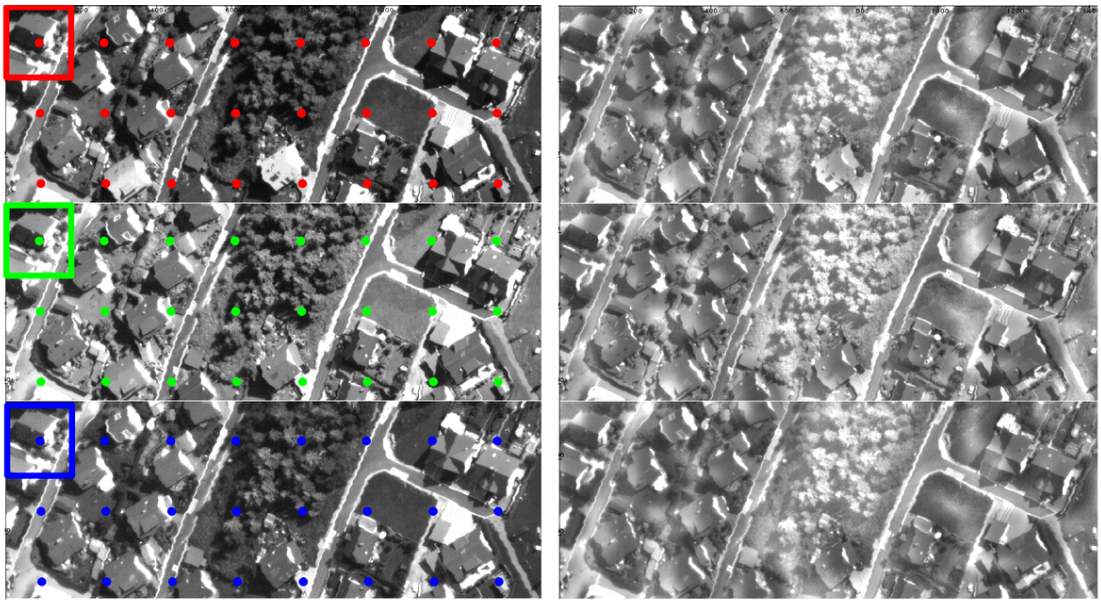

Figure A.4: Visualization of radiometric balancing. **a**: red (upper), green (middle), and blue (lower) band of an RGB line image. The dots represent the centers of the quadratic tiles used for the calculation of the local greyvalue offsets and scale factors. **b**: the corresponding images balanced with the presented approach

In order to perform this radiometric balancing for the whole image, the image is divided into tiles of some tens or hundreds of square tiles. The red, green, and blue squares in Fig. A.4a symbolize the first tile in each band of an RGB line image. For every tile a greyvalue histogram is calculated. In this histogram the greyvalue g_1 is determined by the highest of a small percentage (e.g. 0.1%) of the histogram's lowest greyvalues. Also

the greyvalue g_2 is determined by the lowest of the same percentage of the histogram's highest values. Finally the offset $o = g_1$ and the scale $a = (g2 - g1)/g_max$ are calculated where g_max is the maximum possible greyvalue.

o and a are calculated and saved for the center point (symbolized by the colored dots in Fig. A.4a) of every tile in every band independently. In order to avoid artificial discontinuities in the greyvalues of the images after applying the correction parameters to the greyvalues, both, the offset and the scale, are interpolated via bicubic interpolation between the tile center points. These interpolated correction parameters (o_{interp}, a_{interp}) are then applied to the greyvalues (g) at the corresponding positions, resulting in the corrected greyvalues $g_{corr} = (g - o_{interp}) * a_{interp}$.

The result is shown in Fig. A.4b. Thanks to the radiometric balancing the greyvalues of many large areas become much more similar in the different spectral bands. Although some other areas cannot be corrected appropriately, this is a huge improvement for the determination of corresponding image points.

A.3 List of Abbreviations

DGPS	Differential global positioning system
ECEF	Earth centered earth fixed (coordinate system)
IMU	Inertial measurement unit
GNSS	Global navigation satellite system
GPS	Global positioning system
LSR	Local space rectangular (coordinate system)
NAVSTAR GPS	Name of the global navigation satellite system (GNSS) maintained by the United States government.
NCC	Normalized Cross Correlation
SIFT	Scale Invariant Feature Transform
SLERP	Spherical Linear Interpolation
SURF	Speeded Up Robust Features
WGS	World Geodetic System

Bibliography

Raimundo Almeida-Filho and Yosio E. Shimabukuro. Digital processing of a Landsat-TM time series for mapping and monitoring degraded areas caused by independent gold miners, Roraima State, Brazilian Amazon. *Remote Sensing of Environment*, 79, Issue 1, 2002.

Herbert Bay, Andreas Ess, Tinne Tuytelaars, and Luc Van Gool. SURF: Speeded Up Robust Features. *Computer Vision and Image Understanding (CVIU)*, 110(3):346–359, 2008.

Bryce E. Bayer. Color imaging array. *US patent 3971065*, 1976.

Anko Börner, Heiko Hirschmüller, Karsten Scheibe, Michael Suppa, and Jürgen Wohlfeil. MFC - a modular line camera for 3D world modelling. *Proceedings of Robot Vision, International Workshop RobVis 2008*, pages 319–326, 2008.

Jean-Yves Bouguet. Pyramidal Implementation of the Lucas Kanade Feature Tracker. Description of the algorithm. Technical report, Intel Corporation Microprocessor Research Labs, 2000.

Michael Cramer. Direct geocoding - is aerial triangulation obsolete? *Photogrammetric Week*, pages 59–70, 1999.

Michael Cramer, Dirk Stallmann, and Norbert Haala. High Precision Georeferencing using GPS/INS and Image Matching. In *Proc. of the International Symposium on Kinematic Systems in Geodesy, Geomatics and Navigation, Banff, Alberta, Canada*, pages 453–462, 1997.

Francoise de Lussy, Daniel Greslou, and Lydwine Gross Colzy. Process Line for Geometrical Image Correction of Disruptive Microvibrations. In *International Archives of the Photogrammetry, Remote Sensing and Spatial Information Sciences*, volume XXXVII. part B1, pages 27–34, 2008.

Andreas Eckardt, Bernhard Braunecker, and Rainer Sandau. Performance of the Imaging System in the LH Systems ADS40 Airborne Digital Sensor. In *International Archives of Photogrammetry and Remote Sensing*, volume XXXIII, part B1, pages 104–108, 2000.

Allan Read Eisenman, Carl Christian Liebe, and John Leif Jorgensen. The New Generation of Autonomous Star Trackers. In *Proc. of SPIE*, volume 3221, pages 524–535, 1997.

Stephan Gehrke, Kristian Morin, Michael Downey, Nicolas Boehrer, and Thomas Fuchs. Semi-Global Matching: An Alternative to LiDAR for DSM Generation? In *International Archives of the Photogrammetry, Remote Sensing and Spatial Information Sciences*, volume XXXVIII, part 1, 2010.

Armin Gruen and Li Zhang. Sensor Modeling for Aerial Mobile Mapping with Three-Line-Scanner (TLS) Imagery. In *International Archives of Photogrammetry and Remote Sensing"*, volume XXXIV, part 2, pages 139–146, 2002.

Shubham Gupta, Siddharth Choudhary, and P.J. Narayanan. 3D Reconstruction on GPU: A Parallel Processing Approach. In *Proc. of ECCV 2010 Workshop on Computer Vision on GPUs*, 2010.

Klaus Gwinner, Frank Scholten, Frank Preusker, Stephan Elgner, Thomas Roatsch, Michael Spiegel, Ralph Schmidt, Jürgen Oberst, Ralf Jaumann, and Christian Heipke. Topography of Mars from global mapping by HRSC high-resolution digital terrain models and orthoimages: Characteristics and performance. *Earth and Planetary Science Letters*, 294, Issue 3-4:506–519, 2009.

Norbert Haala, Dirk Stallmann, and Michael Cramer. Geometric Processing Of High Resolution Airborne Scanner Imagery Using GPS-INS And Ground Control Points. In *Proc. Third International Airborne Remote Sensing Conference and Exhibition*, pages 371–378, 1997.

Ludger Hinsken, Scott Miller, Udo Tempelmann, Robert Uebbing, and A. Stewart Walker. Triangulation of LH Systems ADS40 Imagery Using Orima GPS/IMU. In *PCV02*, page A: 156, 2002.

Heiko Hirschmüller. Stereo Processing by Semiglobal Matching and Mutual Information. *IEEE Transactions on Pattern Analysis and Machine Intelligence*, 30(2):328–341, 2008.

Heiko Hirschmüller and Daniel Scharstein. Evaluation of Stereo Matching Costs on Images with Radiometric Differences. *IEEE Transactions on Pattern Analysis and Machine Intelligence*, 31(9):328–341, 2009.

Otto Hofmann. Investigations of the accuracy of the digital photogrammetry system DPS, a rigorous three dimensional compilation process for push broom imagery. In *ISPRS, Com. IV/2*, 1984.

Otto Hofmann. A Digital Three Line Stereo Scanner System. In *International Archives of Photogrammetry and Remote Sensing*, volume 27, pages 206–213, 1988a.

Otto Hofmann. Stereophotogrammetrisches Aufnahme- und Auswerteverfahren. *Patent DE 3219032*, 1988b.

Michal Jama, Chris Lewis, and Dale Schinstock. Stereo Processing Pushbroom Images With Correlated Path Measurements. In *Proc. of American Society for Photogrammetry and Remote Sensing annual conference, Baltimore, MD*, 2009.

Klaus Janschek and Valerij Tchernykh. Optical Correlator for Image Motion Compensation in the Focal Plane of a Satellite Camera. *Space Technology*, 21, Issue 4:127–132, 2001.

Klaus Janschek, Valerij Tchernykh, Serguei Dyblenko, and Grégory Flandin. A Visual Feedback Approach for Focal Plane Stabilization of a High Resolution Space Camera. *at-Automatisierungstechnik 53*, 10:484–492, 2005.

Sultan Kocaman. Investigations on the Triangulation Accuracy of STARIMAGER Imagery. In *Proc. of ASPRS Annual Conference*, 2005.

Franz Leberl, Roland Perko, and Michael Gruber. Color in Photogrammetric Remote Sensing. In *International Archives of the Photogrammetry, Remote Sensing and Spatial Information Sciences*, volume XXXIV, part 7, pages 59–64, 2002.

Rongxing Li, Guoqing Zhou, Nicholas J. Schmidt, Cindy Fwoler, and Grady Tuell. Photogrammetric processing of high-resolution airborne and satellite linear array stereo images for mapping applications. *International Journal of Remote Sensing*, 23(20): 4451 – 4473, 2002.

Manolis I. A. Lourakis and Antonis A. Argyros. The design and implementation of a generic sparse bundle adjustment software package based on the levenberg-marquardt algorithm. Technical report, ICS-FORTH, Heraklion, Crete, Greece, 2004.

David G. Lowe. Distinctive Image Features from Scale-Invariant Keypoints. *International Journal of Computer Vision*, 60(2):91–110, 2004.

Richard Billings Merrill. Color Separation in an Active Pixel Cell Imaging Array Using a Triple-Well Structure. *US Patent 5965875*, 1999.

Timm Olhof. Block triangulation using three-line images. In *Proc. of Photogrammetric Week 1995*, pages 197–206, 1995.

Regis Perrier, Elise Arnaud, Peter Sturm, and Mathias Ortner. Satellite image registration for attitude estimation with a constrained polynomial model. In *Proc. of the 17th IEEE International Conference on Image Processing (ICIP)*, pages 925 – 928, 2010.

Gordon Petrie. Airborne pushbroom line scanners: an alternative to digital frame cameras. *GeoInformatics*, Jan./Feb. 2005:50–57, 2005.

Ralf Reulke, Udo Tempelmann, Dirk Stallmann, Michael Cramer, and Norbert Haaler. Improvement of Spatial Resolution with Staggered Arrays As Used in The Airborne Optical Sensor ADS40. In *Proceedings of the 20th ISPRS Congress*, volume XXXV, pages 1682–1750, 2004.

Serge Riazanoff. SPOT 123-4-5 Geometry Handbook. Technical Report GAEL-P135-DOC-001, SPOT IMAGE, 2004.

George T. Schmidt. INS/GPS Technology Trends. *NATO RTO Lecture Series Low-Cost Navigation Sensors and Integration Technology*, RTO-EN-SET-116:1–1 to 1–18, 2010.

Ralph Schmidt, Michael Spiegel, Christian Heipke, Alexander Dumke, and Gerhard Neukum. Operational determination of tie points and bundle adjustment of HRSC images of the Mars Express Mission. In *International Archives of the Photogrammetry, Remote Sensing and Spatial Information Sciences.*, volume XXXVII, part B4, pages 1025–1030, 2008.

Klaus-Peter Schwarz, Michael A. Chapmann, Elizabeth Cannon, and Patrick Wong. An integrated INS/GPS approach to the georeferencing of remotely sensed data. *Photogrammetric Engineering and Remote Sensing*, 59(11):1667–1674, 1993.

Horst Schwarzer, Anko Boerner, Karl-Heinz Degen, Andreas Eckardt, and Patrick Scherbaum. Dynamic PSF and MTF measurements on a 9k TDI CCD. In *Proc. of SPIE Sensors, Systems, and Next-Generation Satellites XII*, volume 7106, 2008.

ScienceDaily. First satellite map of Haiti earthquake. European Space Agency, January 2010. URL `http://www.sciencedaily.com/releases/2010/01/100114143323.htm`. Retrieved March 24, 2011.

Jianbo Shi and Carlo Tomasi. Good Features to Track. *Proc. of IEEE Conference on Computer Vision and Pattern Recognition (CVPR'94)*, pages 593 – 600, 1994.

Martin Smith, Nikolaos Kokkas, and Khaldoun Qtaishat. Investigation into Self Calibration methods for the Vexcel UltraCam D Digital Aerial Camera. *Jordan Journal of Civil Engineering*, 4(2):95–105, 2010.

Michael Spiegel. Improvement of Interior and Exterior Orientation of the Three Line Camera HRSC with a Simultaneous Adjustment. *International Archives of Photogrammetry, Remote Sensing and Spatial Information Sciences*, 36:161–166, 2007.

Timothy Stryker and Brenda Jones. Disaster Response and the International Charter Program. *Photogrammetric Engineering and Remote Sensing*, 76(1):1342–1344, 2009.

Valerij Tchernykh, Sergei Dyblenko, Klaus Janschek, Klaus Seifart, and Bernd Harnisch. Airborne test results for a smart pushbroom imaging system with optoelectronic image correction. In *Proceedings SPIE Sensors, Systems, and Next-Generation Satellites VII*, volume 5234, pages 550–559, 2003.

Carlo Tomasi and Takeo Kanade. Shape and Motion from Image Streams: a Factorization Method - Part 3: Detection and Tracking of Point Features. Technical Report CMU-CS-91-132, Computer Science Department, Carnegie Mellon University, 1991.

Jürgen Wohfeil and Anko Börner. Optical orientation measurement for remote sensing systems with small auxiliary image sensors. In *International Archives of the Photogrammetry, Remote Sensing and Spatial Information Sciences*, volume XXXVIII, part 1, 2010.

Jürgen Wohlfeil. Determining fast orientation changes of multi-spectral line cameras from the primary images. *To be published as an article in the ISPRS Journal of Photogrammetry and Remote Sensing*, 2011.

Jürgen Wohlfeil and Tilman Bucher. A modular, interactive software-concept for radiometric and geometric correction of airborne and spaceborne linescanner images. *Remote Sensing f. Environmtl. Monitoring, GIS Apps., and Geology IX*, 7478:1E 1–12, 2009.

List of Figures

List of Tables

Selbständigkeitserklärung

Ich versichere, dass ich die Dissertation zum Thema „*Optical Orientation Determination for Airborne and Spaceborne Line Cameras*“ selbständig und ohne unerlaubte Hilfe angefertigt habe. Ich habe die Dissertation an keiner anderen Universität eingereicht und besitze keinen Doktorgrad im Fach Informatik. Die Promotionsordnung der Mathematisch-Naturwissenschaftlichen Fakultät II vom 17.01.2005, zuletzt geändert am 13.02.2006, veröffentlicht im Amtlichen Mitteilungsblatt Nr. 34/2006 ist mir bekannt.

Jürgen Wohlfeil